Master's Thesis

for obtaining the academic degree

Diplom-Ingenieur

Gas-phase hydrophobization of paper

"Changing the contact angle without changing other paper properties"

Philipp Wulz B.Sc.

Technical Chemistry

Institute of Bioproducts and Paper Technology

Handed in at the University of Technology Graz

supervised by

Assoc. Prof. Mag.rer.nat. Dr.rer.nat. Stefan Spirk

Dipl.-Ing. Dr. Sarah Krainer

August, 2020

EIDESSTAATLICHE ERKLÄRUNG

Ich erkläre an Eides statt, dass ich die vorliegende Arbeit selbstständig verfasst, andere als die angegebenen Quellen/Hilfsmittel nicht benutzt, und die den benutzten Quellen wörtlich und inhaltlich entnommenen Stellen als solche gekennzeichnet habe.

Graz, am ....

(Unterschrift)

STATUTORY DECLARATION

I declare that I have authored this thesis independently, that I have not used other than the declared sources / resources, and that I have explicitly marked all material which has been quoted either literally or by content from the used sources.

....

(date) (signature)

ACKNOWLEDGMENT

First, I would like to thank everybody who supported me while this master's thesis and during my whole studies.

I would like to express my gratitude to Dr. Stefan Spirk and Dr. Ulrich Hirn who supported me with their extensive expertise, guidance and patience throughout my whole master's thesis. I am equally grateful to my supervisor Dipl.-Ing. Dr. Sarah Krainer for her help and guidance and especially for providing me a comfortable atmosphere during my thesis work.

Special thanks to Dipl. Ing. Werner Schlemmer who provided me a working station and the vacuum pump in the laboratory.

My gratitude also goes to my colleagues at IPZ and research group Spirk, with whom I had fun at work and during leisure time.

I also thank my fellow student Jakob Dohr, with whom I have learned many hours for many exams, not forgetting the hours-long FIFA sessions which distracted me from learning stress.

Finally, the most special thank goes to my mother, stepfather and whole family, who always supported me throughout my whole time at the university.

ABSTRACT

In inkjet printing, several factors are important for the printing quality. One of the most important properties, besides the printing technology and the ink composition, is the interaction of the used ink with the paper surface and the bulk. In order to be able to investigate the solid-liquid interaction depending on the hydrophobicity of a paper surface, this work explores suitable methods to hydrophobize paper sheets without changing other fundamental paper properties.

An unsized raw paper was sized with different chemicals in gas-phase and the change of the hydrophobicity was investigated with contact angle measurements. The most promising method was the hydrophobization with hexamethyldisilazane, because a high contact angle with water was reached, whereby the other paper properties were not changed. Based on these results the pure influence of the hydrophobicity on the printing behavior could be examined. Due to the silylation the feathering effect of the ink on the paper surface could be minimized in order to create a more uniform printing image.

The unsized raw paper was also treated with a trifluoroacetic anhydride/ acetic anhydride mixture, which led to a higher degree of hydrophobization, but unfortunately the mechanical properties of the paper decreased massively, due to the acidic reaction conditions.

Another method was the palmitoylation with palmitoyl chloride, which results in the highest contact angle change compared to the untreated paper, but due to the high reaction temperature and low pressure needed for the reaction to take place, no further investigations were carried out.

In addition, a gas-phase hydrophobization with alkenyl succinic acid was tried, which did not provide the desired increase in hydrophobicity.

Zusammenfassung

Die Druckqualität beim Inkjetdruck ist abhängig von verschiedenen Faktoren. Die wichtigste Eigenschaft, außer der Druckvorrichtung (des Druckers) und der Zusammensetzung der Tinte, ist die Interaktion der Tinte mit der Papieroberfläche und dem Inneren des Papiers. Um die Abhängigkeit der Interaktion einer Flüssigkeit mit der Papieroberfläche von der Hydrophobierung zu untersuchen, befasst sich diese Arbeit mit der Suche nach einer geeigneten Methode um Papier zu hydrophobieren, ohne dabei andere fundamentale Papiereigenschaften zu verändern.

Unbehandeltes und ungeleimtes Papier wurde durch verschiedene Chemikalien in der Gasphase geleimt und die Änderung der Hydrophobizität wurde mittels Kontaktwinkel-Messungen untersucht. Die vielversprechendste Methode war die Gasphasen-Hydrophobierung mit Hexamethyldisilazan, da ein hoher Kontaktwinkel mit Wasser erreicht wurde, wohingegen die anderen Papiereigenschaften nicht geändert wurden. Aufgrund dieser Resultate konnte der reine Einfluss der Hydrophobizität auf das Druckverhalten untersucht werden. Durch die Silylierung konnte der Feathering-Effekt der Tinte auf der Papieroberfläche minimiert werden, um ein gleichmäßigeres Druckbild zu erzeugen.

Das unbehandelte Rohpapier wurde außerdem mit einer Mischung aus Trifluoressigsäureanhydrid und Essigsäureanhydrid behandelt, wodurch eine Erhöhung des Kontaktwinkels erzielt wurde. Allerdings wurden die mechanischen Eigenschaften des Papiers, aufgrund der sauren Reaktionsbedingungen, stark verringert.

Eine weitere Methode war die Palmitoylierung mit Palmitoylchlorid, welche den höchsten Kontaktwinkel aller Methoden im Vergleich zum unbehandelten Papier aufwies. Aufgrund der hohen benötigten Reaktionstemperatur und des niedrigen Drucks wurden jedoch keine weiteren Nachforschungen angestellt.

Schlussendlich wurde eine Gasphasen-Hydrophobierung mit Alkenylbernsteinsäure versucht, die aber nicht die gewünschte Erhöhung der Hydrophobizität erzielte.

Table of content

1 Introduction and motivation

Nowadays, inkjet printing is an easy, quick and low cost method to bring electronic information on a piece of paper [1]. The quality of the printouts is depending on various factors, for instance the printer, the ink and the paper [2] and combination out of these factors.

The liquid-paper interaction, also known as wetting and penetration, is one of the most crucial parts in printing industry, especially for high-speed-inkjet (HSI) printing. A certain amount of the ink carrier liquid should penetrate the paper, while the ink dyes should stay at the surface without lateral spreading to achieve a high printing quality. Raw and untreated paper absorbs too much liquid to write and print in a high quality and therefore the paper sheets are modified during the papermaking process. The paper sheets can be coated with a primer, which is for instance a binary salt ($CaCl_2$), to enhance the color density [3]. Another way is to add sizing agents, such as AKD or ASA, for an internal sizing to hydrophobize the paper to reduce penetration speed and spreading [4, 5].

The main problem with these techniques is, that not only wettability is changed but also the porosity of the paper. In order to be able to investigate the impact of hydrophobicity on paper-liquid interaction, it is necessary to adjust the degree of hydrophobization and at the same time maintain all paper properties. To achieve this goal gas-phase hydrophobization can be used. Thereby, the sizing agent is evaporated in a closed vessel and reacts with the hydroxyl groups of the cellulose to form a hydrophobic surface.

The aim of this thesis is to explore gas-phase hydrophobization methods without affecting other paper properties. First, different sizing agents for the gas-phase hydrophobization were tested and then the modified paper sheets were examined for changes in its mechanical and optical properties. Finally, the best method was selected for further researches.

Theoretical background

2 Paper production

In paper technology, many different types of paper and cardboards are known. All these kinds of cellulose containing materials are produced with different kinds of process techniques, raw materials, fillers and chemical additives to obtain the special properties needed in various applications. As described in the paper lexicon [6] there are four major groups, in which more than 3000 paper grades are listed:

a) Graphic paper (print and writing paper)
b) Wrapping paper and cardboards
c) Hygiene paper
d) Technical paper and special paper

In this thesis the main focus lays on the first major group, which contains printing and writing paper types. For this thesis an unsized and untreated paper, which is also known as plain paper is used.

2.1 Fibrous raw materials

The basis material of paper production is paper pulp, which is divided into primary fibers and secondary fibers. Primary fibers are produced out of herbal raw materials, especially wood, while secondary fibers are made from wastepaper. Furthermore, a distinction is made in the case of primary fibrous materials between chemically disrupted cellulose and mechanically fibrillated wood pulp. On the one hand, the yield in chemical pulping is between 45 % and 55 % and on the other hand, wood pulp obtained from mechanical fibrillation is obtained in a yield of 80 to 95 %. [7, 8]

The global pulp production in 2017 amounts to 184 million tons made from wood, which is approximately 80% higher than in 1980. In contrast to this, the use of wastepaper in paper production increased from 54 to 199 million tons demonstrating that, recycling has got more important in the last 40 years [9].

2.2 Paper additives

Paper contains a large variety of additives either to improve the finished paper sheets or to help in the process of papermaking. The additives are divided into two big main groups, called control additives and functional additives. First mentioned are biocides, drainage aids, retention aids, defoamers and pitch control agents to improve the process of papermaking. Functional additives are fillers, adhesives, dyes and internal sizing agents. Both types of paper additives are added to the pulp slurry before the papermaking process starts on the paper machine. [10]

For further information on paper additives please refer to "Handbook of Pulp and Papermaking" [10]. Since this thesis deals with hydrophobization methods of paper, internal sizing methods will be discussed in detail in the next chapter.

2.3 Paper sizing: Increase of the hydrophobicity of paper

Cellulose can be easily wetted by water, because of its high hydrophilicity due to the hydroxyl groups. Therefore, the contact angle of water on an unsized paper is very low. With the use of a sizing agent, the cellulose gets hydrophobized, which leads to a higher contact angle (>90°) between the solid and the polar liquid phase. The higher contact angle is reached because the surface energy of the solid phase gets decreased. In general, sizing agents are amphiphilic, consisting of a polar head group, which binds to the cellulosic hydroxyl groups or through a linker, for instance alum and an unpolar tail, as illustrated in Figure 1. [10]

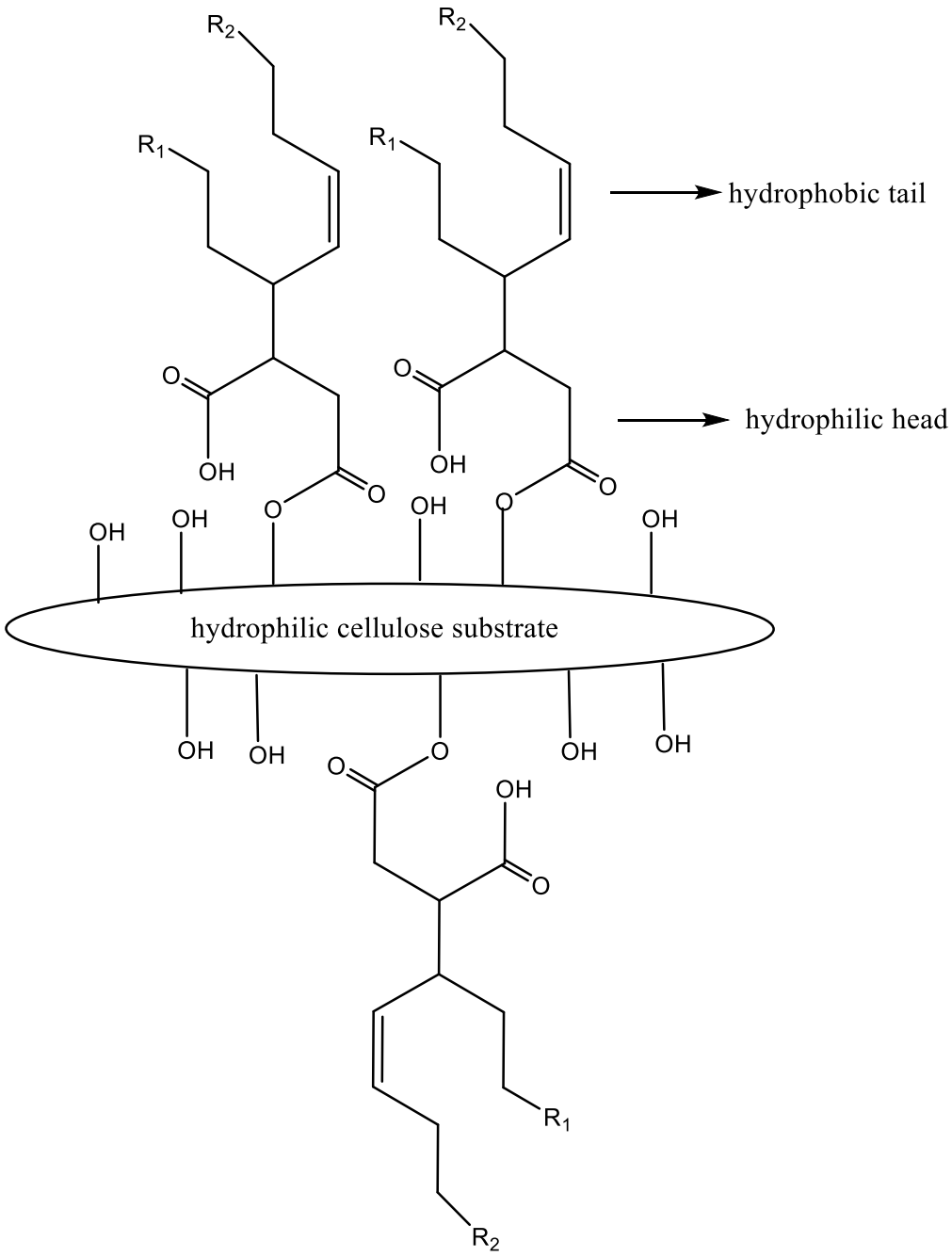

Figure 1: Schematic depiction of an amphiphilic sizing agent (AKD) on a cellulose substrate.

2.4 Internal/ Bulk sizing

Traditionally, paper sizing was made under acidic conditions with rosins and alum and the major rosin source was wood itself [12]. Rosins are not a single compound, but rather a mixture of closely related materials of wood pitch. One of the major components is abietic acid [13]. Abietic acid (shown in Scheme 1) has one carboxylic acid group, which anchors to the hydroxyl groups of the cellulose in paper and three six membered carbon-hydrogen rings. Because of these rings the major part of the molecule is water-repellent.

Nowadays when rosin sizing is used, abietic acid gets modified to the reaction shown below (Scheme 1), where the initial product contains an additional ring, which opens subsequently when it gets in contact with water, forming a second and third carboxylic acid group. These additional groups lead to more anchoring sides and a higher storage ability of the improved rosin. [14]

Due to some disadvantages in acidic rosin sizing, for instance the phenomenon that paper produced with this technique becomes brittle with long storage times, some experts made experiments to find out which factors lead to this ageing effect. In 1989 Barret [15] found out that there is a strong correlation between the pH of the paper and its ageing behavior over time. Moreover, Arney and Chapdelaine [16] did some tensile strength experiments while heating up the paper to enhance the ageing process, to show that the acidity contributes to the embrittlement.

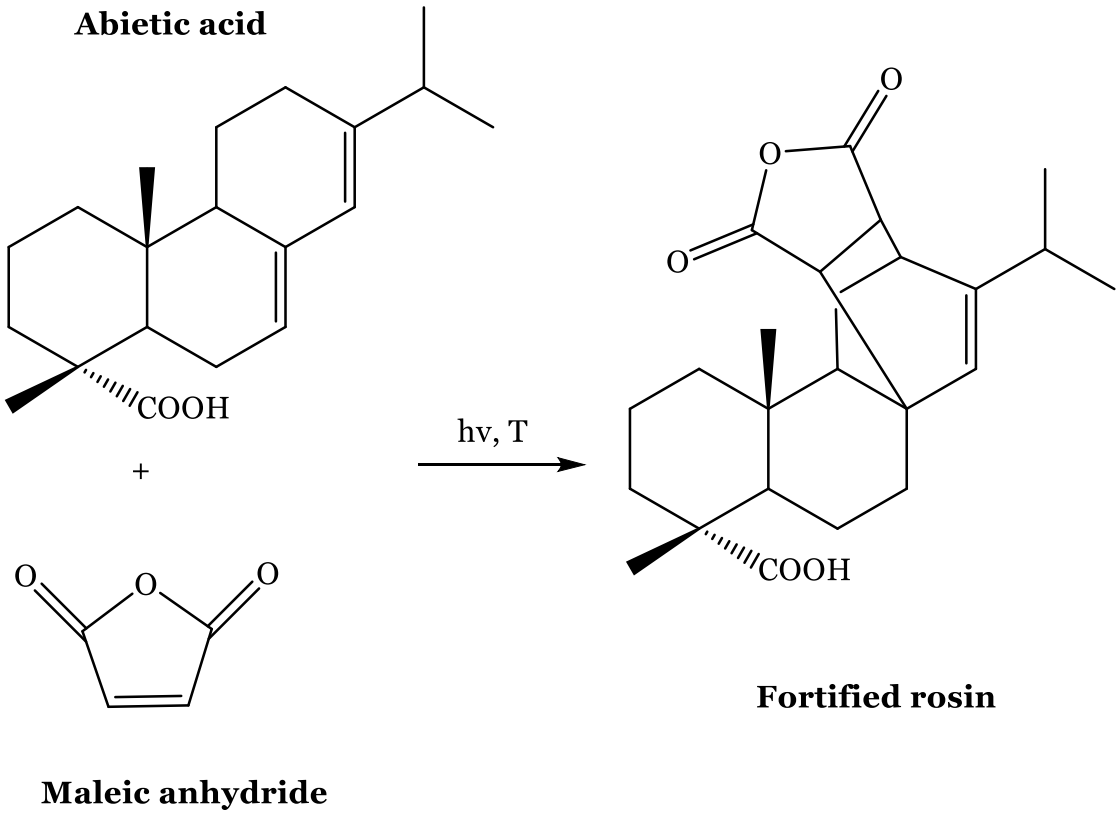

Scheme 1: Major component of wood rosin for internal acidic sizing (abietic acid) and the reaction with maleic anhydride to form fortified rosin.

Attributable to this ageing effect a new sizing method was invented, which is widely used nowadays. The acidic reaction conditions with rosin sizing was replaced by

neutral or alkaline sizing methods. The problem was that rosin sizing with alum fixation did not work anymore because at pH 6 all the aluminum becomes converted to aluminum floc, which is unable to react with a rosin soap (see Equations 1-3). For effective sizing a minimum of bivalent metal ions is necessary to anchor the rosin on the paper`s surface. [14]

$$Al^{3+}(aq) + OH^- \rightarrow Al(OH)^{2+} \quad (1)$$

$$13Al^{3+}(aq) + 32OH^- \rightarrow {Al_{13}(OH)_{32}}^{7+} \quad (2)$$

$$Al^{3+}(aq) + 3OH^- \rightarrow Al(OH)_3 \quad \text{(alum floc)} \ (3)$$

Therefore, cationic rosin formulations got invented and Nitzman and Royappa [17] used cationic polymers for the stabilization of rosin acid-free sizing agents. The emulsion used, got stabilized by polymers called polyamidoamine-epichlorohydrin, which is a wet-strength resin. Successful sizing has been done in a pH range of 5 to 6.5 and even in alkaline conditions, because of the addition of cationic charges from the polymers. This leads to a fixation of the resin on the fiber surfaces. [14], [17]

The first completely alkaline sizing agent was alkylketene dimer (AKD), which is a waxy compound, produced out of fatty acids found in vegetable oils [18]. Chemically, AKD is produced by dimerization of stearoyl chloride [19]. AKD needs to be emulsified in presence of cationic starch or other cationic polymers, before it can be used as sizing agent in a paper machine, but AKD is rather unreactive, which allows a purchase of ready-to-use AKD emulsions [4]. In Scheme 2 the reaction of AKD with cellulose and the unwanted side reactions can be seen.

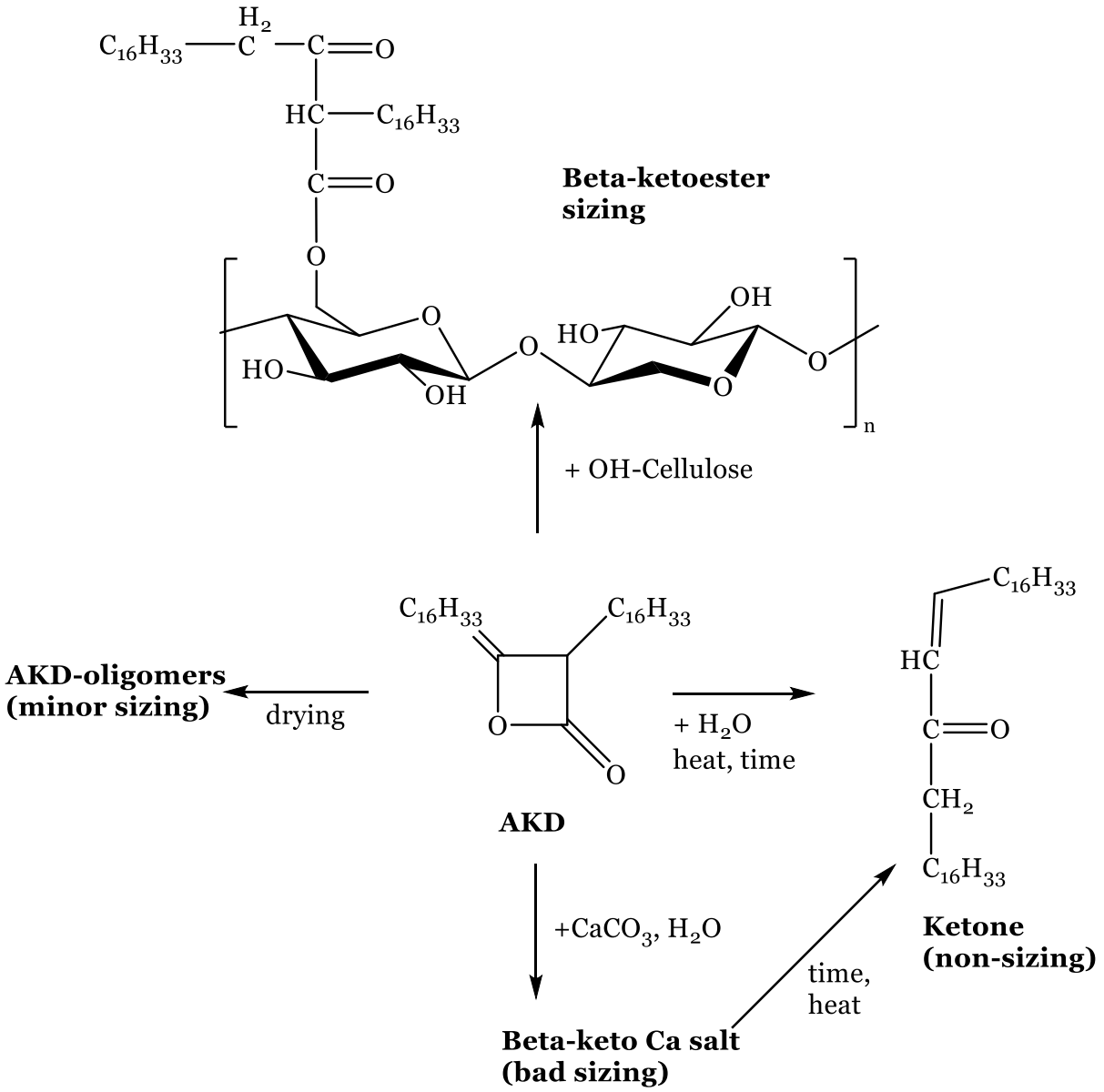

Scheme 2: Sizing mechanism with AKD and possible side reactions affecting the sizing efficiency.

To achieve an increase in hydrophobicity, or in other words an increase in resistance to aqueous fluids, AKD has to form beta-keto ester bonds to the cellulose. Hydrolysis products (ketones) are not able to size a paper sheet. These hydrolysis products are formed in the presence of water and the $CaCO_3$ filler at increased temperature. In addition AKD is able to form oligomers, which are no efficient sizing agents. [14]

The second widely used sizing agent in a neutral or slightly alkaline medium is alkenylsuccinic anhydride (ASA), which is produced by the reaction of maleic anhydride with cracked olefins, which have chain lengths of about 14 to 20 carbon atoms. ASA was first introduced in the 1960s by Wurzburg and Mazzarella [5] and is the most used sizing agent in the USA. [13, 19]

ASA products are water insoluble liquids and have to be emulsified with cationic starch before the introduction in the papermaking machine takes place. After adding the emulsion into the paper machine, ASA has to uniformly cover the fibers and later ASA reacts with the hydroxyl group of the cellulose to from an ester bond. [20] The bond formation of ASA and cellulose and the hydrolysis reaction are illustrated in Scheme 3.

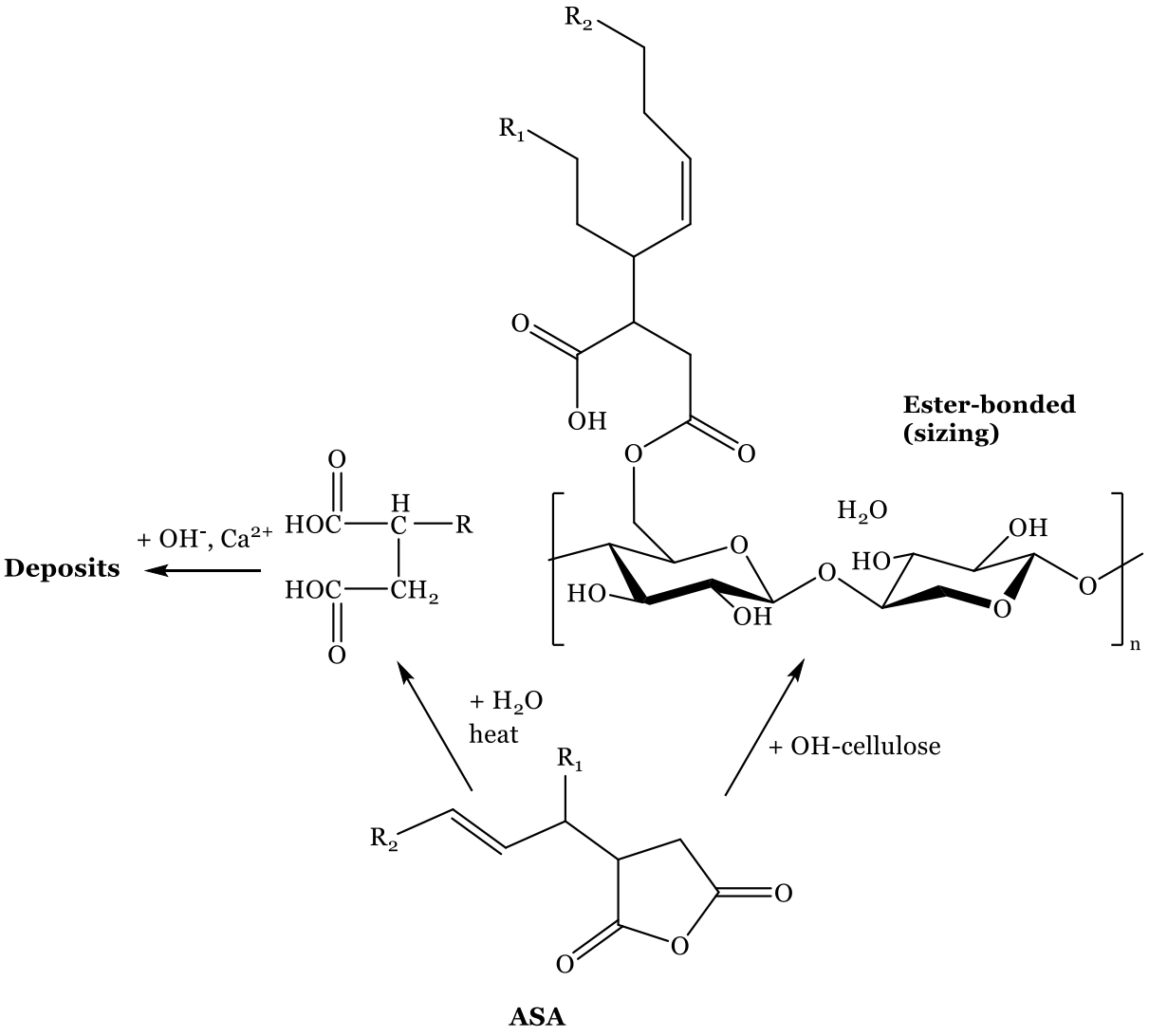

Scheme 3: Sizing mechanism with ASA and possible side reaction affecting the sizing efficiency (hydrolysis).

Hydrolysis reactions during paper making cannot be prevented, because of the water uptake during emulsification, storage and especially in the paper making machine. The hydrolysis product, often a calcium or magnesium salt of the diacid, forms sticky deposits on the parts of the paper machine. Moreover, these hydrolysis products are decreasing the sizing efficiency. [4]

2.5 Surface sizing

Surface sizing can be achieved by deposition of a film of a hydrophobic material (e.g. cationic starch) on the surface of the paper. The purpose is to enhance the resistance to penetration of liquids, for better surface properties and to improve physical properties of the paper, especially tensile strength. [21] Compared to bulk sizing, less sizing agent is required, but an additional sizing unit (size press) has to be in the paper machine, which leads to higher costs and a higher energy demand [22].

3 Wetting and Penetration

3.1 Wettability of a surface

To achieve a high printing quality, especially in high speed inkjet printing, the penetration of the ink into the paper and the spreading of the ink drop at the paper surface are crucial. At first, the ink wets the surface and then the ink penetrates into the capillary network of the paper. [23]

By changing the paper properties, for instance the hydrophilicity or pore structure, wetting and penetration can be tuned to achieve a high printing quality. When using an uncoated inkjet paper, which is very cheap in production, the ink droplets spread along the paper fibers and penetrate into the bulk [24]. This can lead to a strike through and poor optical density after printing, in particular with color printings [25]. In contrast, using a coated paper, ink droplet penetration into the bulk is decreased, which causes increased drying times, increased smearing [25] and higher dot gain [26]. Because of these controversies, many research groups are investigating ink-paper interactions to find the perfect paper coatings for a high print quality [27, 28].

3.1.1 Wettability of a smooth substrate

As described in Chapter 3 the first interaction between a fluid and the substrate is wetting. Wetting on a smooth substrate was first described by Young in 1805 [29], where the wetting behavior is expressed by the surface energy/tension vectors in the three-phase contact point between the liquid, gas and solid, as depicted in Figure 2. These three surface energies or tensions can be related to each other by introducing the contact angle (θ) as another important criterion to describe the wetting phenomenon. It is influenced by the liquid surface tension (γ_{lg}), the interfacial surface tension between the solid and the liquid (γ_{sl}) and by the surface energy of the substrate (γ_{sg}) surrounded by air. [29] The contact angle is defined as the angle between the surface of the liquid and the outline of the contact surface [30].

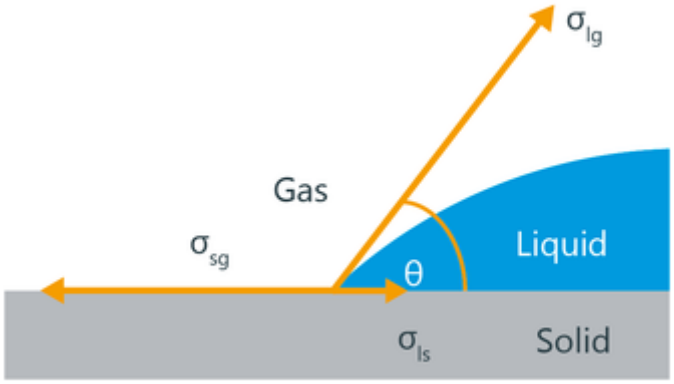

Figure 2: Liquid drop on a solid medium, where a tangent is applied to the drops outline at the three-phase contact point (liquid, solid and gas phase). The contact angle (θ) is determined by the three-surface energy/ tension vectors (γ_{lg}, γ_{sl}, γ_{sg}). Picture taken from [30].

As depicted in Figure 3, weak sizing leads to contact angles below 90 degree (θ < 90°), which results in a good wetting behavior, with a good spreading of the drop on the substrate. Furthermore, if θ = 0, complete wetting occurs and a liquid film forms on the substrate. Contact angles higher than 90 degree (θ > 90°) leads to a bad wetting behavior, without liquid spreading on the surface. [31]

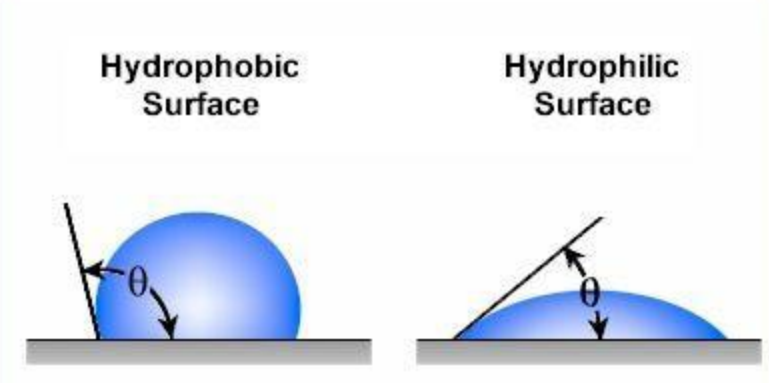

Figure 3: left side: bad wetting with θ > 90°, while placing a water droplet on a hydrophobic surface; right side: good wetting (θ < 90°) with drop spreading over the surface, while placing a water droplet on a hydrophilic surface. Picture taken from [32].

On a chemically homogenous and smooth surface and with the use of a pure liquid Young's equation [29] can be used to describe the equilibrium state of the contact angle and the three surface energies/tensions between the drop and the solid substrate (see Equation 4).

$$\gamma_{sg} = \gamma_{sl} + \gamma_{lg} \cos(\theta) \quad (4)$$

γ_{sg} = surface energy of the substrate sourrounded by a gas (air) [N/m]

γ_{sl} = interfacial surface tension between the solid and the liquid [N/m]

γ_{lg} = liquid surface tension [N/m]

θ = contact angle [°]

One drawback of Young's explanation of the wetting phenomena is, that hardly any completely smooth and chemically homogenous surface exists. This surface roughness is influencing the surface energies/ tensions and therefore the contact angle [33].

3.2 Influence of roughness on the wettability

As mentioned in Chapter 3.1.1 Young's equation is only valid for perfectly smooth and chemically homogenous substrates. Due to uneven surfaces, the liquid-solid interaction gets complicated and many researchers tried to investigate the influence of the roughness on this interaction [34]. Liquid drops on rough surfaces create an apparent contact angle, which differs from the contact angle on a smooth surface, as described by Young [35]. Nowadays, two classic models are available to describe the liquid-solid interaction on rough surfaces: Wenzel [36] first described this phenomenon in 1936 and Cassie and Baxter [37] found a second method in 1944 (see Figure 4). The Wenzel state differs from the Cassie-Baxter state in that, the liquid drop interacts in another way caused by the roughness of the solid surface.

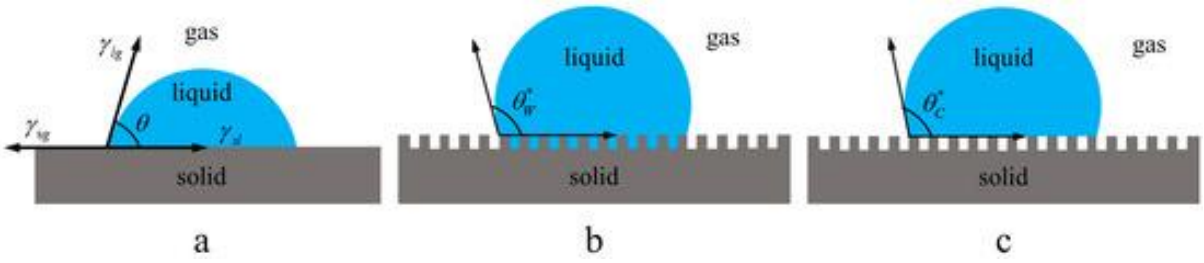

Figure 4: Three different wetting models: (a) Wetting of a smooth and chemically homogenous surface according to Young; (b) Wetting of a rough substrate according to the Wenzel state; (c) Wetting of a rough surface according to the Cassie-Baxter state. Picture taken from [38].

3.2.1 Wenzel state

Wenzel [36] stated (as depicted in Figure 4b), that the liquid placed on a rough surface flows into the valleys and adapts to the roughness. Therefore, no air is encapsulated between the drop and the surface.

Moreover, he said that a liquid, which favors wetting, has an enhanced wettability on a rough surface. In the same sense, a bad wetting surface increases this resistance with increasing roughness. This increase or decrease in the wetting ability is due to the increase in surface area with a higher surface roughness. [35]

The apparent contact angle on a fully wetted, chemically homogenous and rough surface is given by the Wenzel equation (see Equation 5).

$$\cos(\theta_W) = r \cdot \cos(\theta) \tag{5}$$

where θ_W is the Wenzel angle, θ is the contact angle on a smooth surface of the same material expressed by Young and r is the roughness factor, which is given by:

$$r = \frac{actual\ surface\ area}{projected\ surface\ area} \tag{6}$$

The Wenzel state describes the wetting behavior for rough surfaces, but not for porous surfaces and therefore, Cassie and Baxter invented a new method to describe the apparent contact angle, especially in natural clothing.

3.2.2 Cassie-Baxter state

Cassie and Baxter [37] analyzed the rain resistance of porous surfaces for example bird feathers or clothing. When a liquid is placed on a porous surface, the liquid does not flow into the pores and air pockets are formed, which create a composite-like interface, depicted in Figure 4c.

The apparent contact angle in the Cassie-Baxter state is determined by the two area fractions of the contact area under the liquid drop, which are the solid and air fraction. Therefore, the general equation for the apparent contact angle (θ_{app}) is [35, 39]:

$$\cos(\theta_{app}) = f_1 \cdot \cos(\theta_1) + f_2 \cdot \cos(\theta_2) \tag{7}$$

where f_1 and f_2 ($f_1 + f_2 = 1$) are the area fractions and θ_1 and θ_2 are the contact angles of the solid-liquid-air interface. Because of the area fraction, which is trapped between the drop and the solid (air) the cosine of 180° equals -1. With an insertion in Equation 7, the Cassie-Baxter equation can be expressed as [35]:

$$cos(\theta_{CB}) = f_1 \cdot \cos(\theta) + (f_1 - 1) \tag{8}$$

θ_{CB} is the Cassie-Baxter angle, f_1 the solid area component and θ is the contact angle on a smooth surface of the same solid material [35].

3.2.3 Critics on Wenzel and Cassie-Baxter state

Till today it is not completely clear when Wenzel's and Cassie-Baxter's wetting models of rough surfaces are valid. On the one hand, both methods laid the foundations for understanding wetting on rough and chemically heterogenous surfaces [40]. But on the other hand, Gao and McCarthy [41] argued that the contact angle behavior is caused by the liquid-solid interaction at the three-phase point and the other area between the drop and the substrate does not affect it. They proved their statement with an experiment, where they prepared three types of two-component surfaces, which have spots of a different structural or chemical behavior in a surrounding field. Moreover, they also refer to Extrand [42] who stated that contact angles are only determined by the three-phase point interactions and not by the interfacial contact area on a heterogenous surface. It must be noted that all measurements and calculations were done with advancing and receding contact angles and furthermore with the contact angle hysteresis, which is defined as:

$$\Delta\theta = \theta_{adv} - \theta_{rec} \tag{9}$$

where θ_{adv} is the advancing contact angle, θ_{rec} is the receding contact angle and $\Delta\theta$ is the contact angle hysteresis. The advancing contact angle is reached by adding the same liquid to a drop on a surface till the contact angle does not change anymore. In contrast, the receding contact angle is reached by removing liquid from a placed drop till the contact angle does not change anymore.

Earlier, Bartell and Sheppard [43] showed that glycerol gives an advancing contact angle of 98° on a smooth and homogenous paraffin surface. After they roughened the surface, they got a contact angle of 148°. However, by advancing the drop until its contact line reached the smooth surface again, the contact angle changed back to 98°, although the most liquid-solid interface was rough. [43]

Some months after Gao and McCarthy's thesis [41], that Cassie and Baxter were wrong, McHale [44] published an article, where he made theoretical assumptions under which the Wenzel and Cassie-Baxter states are valid. He stated, that the roughness factor, introduced from Wenzel and the surface fractions from Cassie-Baxter must be seen as

global parameters of the surface and not as parameters of the surface beneath the contact line of the placed liquid. [44]

In 2008, also Marmur [40] discussed the validity of Wenzel's and Cassie-Baxter's equations, in terms of the most stable contact angle. He said, that both equations are valid, if the drop size is large enough compared to the wavelength of roughness or chemical heterogeneity [40].

3.3 Determination of the solid surface energy γ_{sg}

Taking a look at Young's equation (equation 4) [29], where the contact angle (θ) of a liquid drop on a smooth and chemically homogenous surface is determined by the solid surface energy (γ_{sg}), solid-liquid interface tension (γ_{sl}) and the liquid surface tension (γ_{lg}), only two parameters of the equation can be measured by an experimental approach. These are the contact angle (θ) and the liquid surface tension (γ_{lg}). Therefore, Dupre [45] introduced the concept of reversible cohesion work ω_{coh} and adhesion work $\omega_{adh.}$ The adhesion work is defined as the work, which must be done to separate two adjacent phases [46]. In a wetting process, it is the energy which is released [46]. While wetting a surface by a liquid, the two earlier existing phase boundaries disappear and energy, related to the surface tensions (γ_1 and γ_2) is released. At the same time a work to form the interfacial tension (γ_{12}) must be done [46]. The work of adhesion ($\omega_{adh,\,sl}$) of a liquid on a surface is given by equation 10:

$$\omega_{adh,sl} = \gamma_1 + \gamma_2 - \gamma_{12} \tag{10}$$

Furthermore, Adam [47] stated that the Young's equation can also be written with reference to the work of adhesion (ω_{adh}), contact angle (θ) and the surface tension of the liquid (γ_1) in the following way:

$$\omega_{adh,sl} = \gamma_l(1 + cos\theta) \tag{11}$$

Equation 11 is nowadays known as the Young-Dupre equation [48] and with the aid of the work of Owens and Wendt [46], Rabel [50] and Kaelble [51] the surface energy of the substrate can be calculated, by measuring the contact angle and the liquid surface tension.

3.3.1 Owens-Wendt-Rabel-Kaelble (OWRK) method

The OWRK method is an often used method in the paper industry for the determination of the surface energy by measuring the contact angle of two or more

liquids with different polarities [52]. The OWRK method was developed, based on earlier work of Fowkes [52], [53] who recognized that surface tensions of liquids and the surface energy of solids can be split up into partial components [54]. These partial components are addressed to the impact of the different molecular interactions [54]. For instance, the liquid surface tension of liquids is a sum of its polar γ_l^p (from hydrogen bonds) and dispersive forces γ_l^d (equation 12).

$$\gamma_l = \gamma_l^p + \gamma_l^d \tag{12}$$

With this knowledge and Young's equation the following equation for the interface tension (γ_{sl}) between the liquid and the solid can be formed:

$$\gamma_{sl} = \gamma_{sg} + \gamma_{lg} - 2 \cdot \sqrt{\gamma_{sg}^d \cdot \gamma_{lg}^d} \tag{13}$$

where γ_{sl} is the internal tension between the solid surface and the liquid, γ_{sg} is the surface energy of the solid and γ_{lg} is the liquid surface tension. As noted in equation 12, *d* is indicating the dispersive part of the surface energy/tension. Equation 13 is only valid when a saturated hydrocarbon liquid is used, because with them only dispersive forces are present. [55]

As mentioned before, the surface energy can only be calculated by measuring the contact angle of two liquids of different polarity. Therefore equation 13 can be extended by the polar fraction:

$$\gamma_{sl} = \gamma_{sg} + \gamma_{lg} - 2 \cdot \sqrt{\gamma_{sg}^d \cdot \gamma_{lg}^d} - 2 \cdot \sqrt{\gamma_{sg}^p \cdot \gamma_{lg}^p} \tag{14}$$

where *p* indicates the polar part of the surface energy/tension [49].

A combination of the Young-Dupre equation with equation 14 gives the final equation of the OWRK-method, as shown in equation 15.

$$\gamma_{lg} \cdot (1 + cos\theta) = 2 \cdot \sqrt{\gamma_{sg}^d \cdot \gamma_{lg}^d} - 2 \cdot \sqrt{\gamma_{sg}^p \cdot \gamma_{lg}^p} \tag{15}$$

By rearrangement of equation 15, equation 16 can be written as:

$$\frac{\gamma_{lg} \cdot (1 + cos\theta)}{2 \cdot \sqrt{\gamma_{lg}^d}} = \sqrt{\gamma_{sg}^d} + \sqrt{\gamma_{sg}^p} \cdot \sqrt{\frac{\gamma_{lg}^p}{\gamma_{lg}^d}} \tag{16}$$

With equation 16 and contact angle measurements of at least two liquids with a big difference in polarity the surface energy of the substrate can be determined. It has to be noted, that the polar and dispersive fraction and its sum, of the liquid have to be known in advance.

To determine the surface energy, the known parameter (θ, γ_{lg}^{p}, γ_{lg}^{d}) are inserted into equation 16 to get at least two points in an OWRK-plot, depicted in Figure 5. In an OWRK-plot $\frac{\gamma_{lg}\cdot(1+cos\theta)}{2\cdot\sqrt{\gamma_{lg}^{d}}}$ is plotted against $\sqrt{\frac{\gamma_{lg}^{p}}{\gamma_{lg}^{d}}}$ and a linear regression is made. The y-intercept is $\sqrt{\gamma_{sg}^{d}}$ and the slope equals to $\sqrt{\gamma_{sg}^{p}}$. [54]

According to equation 17 the total surface energy can be calculated:

$$\gamma_{sg} = \gamma_{sg}^{p} + \gamma_{sg}^{d} \tag{17}$$

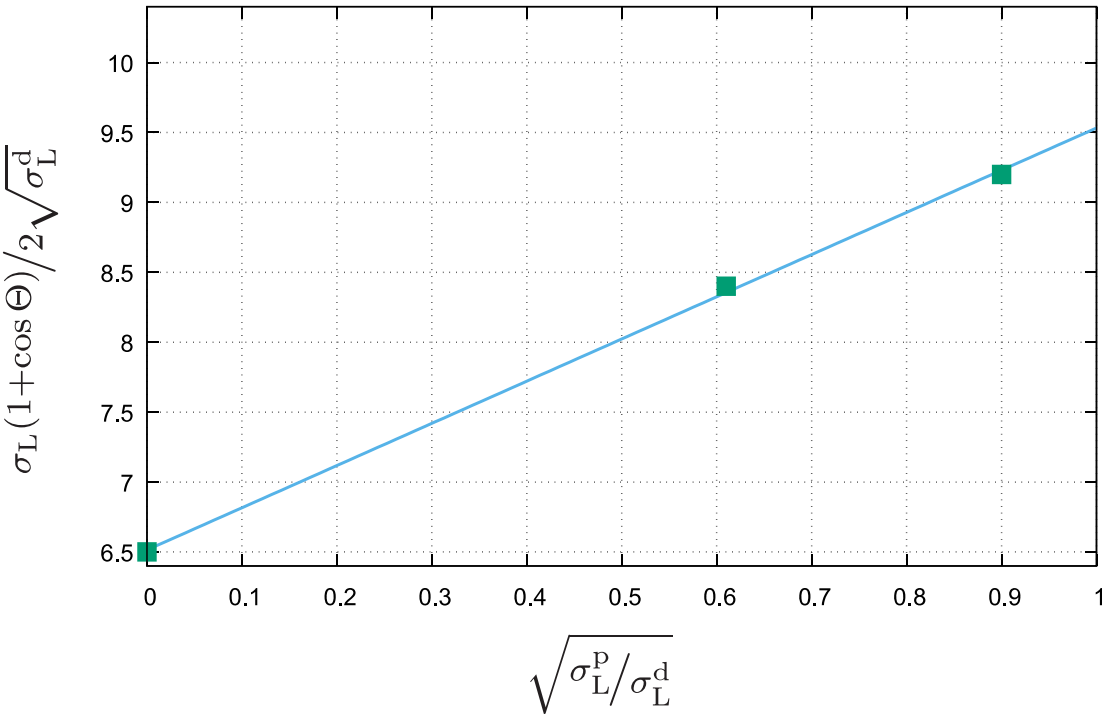

Figure 5: Schematic depiction of an OWRK-plot: the green dots represent the x and y-values of three different liquids with different polarity and known liquid surface tensions. The blue line (linear regression) is used to read the y-interception for $\sqrt{\gamma_{sg}^{d}}$ and the slope for $\sqrt{\gamma_{sg}^{p}}$. Picture taken from [56].

3.4 Liquid penetration in porous substrates

After wetting of the solid surface, the liquid starts to penetrate the porous structure of the substrate. The pores, which arise within the cellulose fiber network, act as cylindrical capillaries, which transport the liquid through the porous material [57]. The capillary pressure (ΔP) of a liquid in a spherical capillary is described by the Laplace equation, which is shown in Equation 18:

$$\Delta P = \frac{2\gamma_{lg}}{R} \tag{18}$$

where γ_{lg} is the surface tension of the liquid and R is the radius of the meniscus. The meniscus will have a hemispherical shape, if the radius of the capillary r is equal to the radius of meniscus R, as depicted in Figure 6. [58]

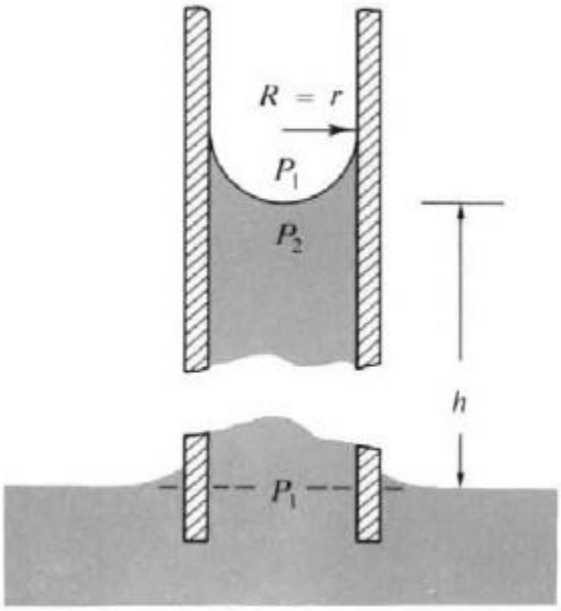

Figure 6: Capillary rise of a liquid in a cylindrical pore building out a hemispherical meniscus with an radius of R, which is equal to the radius of the pore r. P1 refers in general to the atmospheric pressure and P2 is the liquid pressure. Picture taken from [58].

In addition, the contact angle (θ) between the fluid and the capillary wall plays an important role in liquid penetration, because it determines the shape of the meniscus. Therefore, the radius of the curvature of the meniscus R is determined by $R = r/\cos\theta$ as illustrated in Figure 7 [58]. With this approach the Young-Laplace equation can be written as:

$$\Delta P = \frac{2\gamma_{lg}\cdot\cos\theta}{r} \tag{19}$$

Assuming the liquid is water, the contact angle on a hydrophilic substrate is below 90° (θ < 90°) and thus gives a positive capillary pressure, which leads to a spontaneous penetration of the liquid into the pores. In contrast a hydrophobic substrate (θ >90°) leads to a negative capillary pressure and no spontaneous penetration into the capillaries takes place. [58, 59]

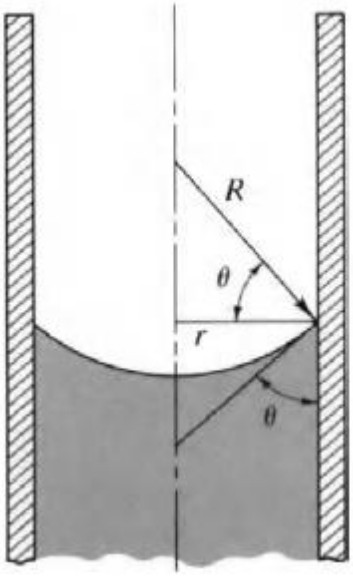

Figure 7: Capillary rise of a fluid in a pore determined by the contact angle θ between the fluid and the pore wall Picture taken from [58].

3.4.1 Lucas-Washburn model of penetration

The capillary rise and therefore the liquid penetration in porous substrates can be determined experimentally as described in Section 3.4. Another approach is the introduction of a model system, which describes the pore system in a simplified way [54]. The most used way to describe such a system is the Lucas-Washburn model of penetration, which is derived from the Poiseuille law, which can be seen in Equation 20. [57, 60]

$$v = \frac{dH}{dt} = \frac{\Delta P \cdot r^2}{H \cdot \eta \cdot 8} \tag{20}$$

In Poiseuille's capillary flow, H represents the penetration length [m], t is the time [s] and v is the laminar flow [m/s] of a liquid in a cylindrical capillary with a known radius r [m]. Moreover, η is the dynamic viscosity of the liquid [Ns/m²] and ΔP is the capillary pressure [Pa], which is the driving force for the penetration of a liquid in a capillary of

a porous substrate. By substitution of ΔP by the Young-Laplace equation (Eq. 19) and integration the Lucas-Washburn equation (Equation 21) can be written as [57, 60]:

$$H = \sqrt{\frac{\gamma_{lg} \cdot r \cdot cos\theta}{2\eta}} \cdot \sqrt{t} \tag{21}$$

As seen in Equation 21, the Lucas-Washburn equation describes the penetration length H of a liquid into a cylindrical capillary during a penetration time t. The penetration length is determined by the liquid surface tension γ_{lg}, the pore radius r, the contact angle of the liquid with the capillary wall (θ) and the viscosity of the liquid. Moreover, H is proportional to $\sqrt{t}$.

Although, the model of Lucas-Washburn can be used in many cases to describe the liquid penetration in porous substrates it should be considered that in reality the pores of porous substrates do not have an ideal cylindrical shape and moreover the capillaries can potentially to overlap [61]. Nevertheless, many research groups use the Lucas-Washburn model, due to its simplicity and the knowledge from experiments that the penetration depth is very often proportional to the square root of the penetration time [61, 62].

4 Chemical vapor deposition (CVD)

To coat a substrate and to change its properties many different processes are known, such as electrochemical plating, conversion coatings, spray coating, spin coating, sol-gel coating, physical vapor deposition (PVD) and chemical vapor deposition (CVD) [63].

As mentioned in Chapter 2.2 paper sizing is mostly done by adding an emulsion of a rosin, AKD or ASA to the pulp slurry, which causes changes not only in hydrophobicity but also in porosity and other paper properties, for instance tensile strength or optical properties. To avoid these changes chemical vapor deposition of a hydrophobization agent could be a promising sizing method.

4.1 Principle of CVD

Chemical vapor deposition is based on the reaction of a gaseous reactant in a vacuum chamber on or near a heated or non-heated substrate with the aim to produce coatings of highly pure materials at nanometer or atomic scale [64]. Moreover CVD is a non-line-of-sight method, compared to PVD or electroplating, which means that also holes and trenches, rather than flat surfaces can be coated in an effective way [65].

A CVD process can be described in seven steps containing mass transport, adsorption/desorption processes and chemical reactions as depicted in Figure 8 [66], [67].

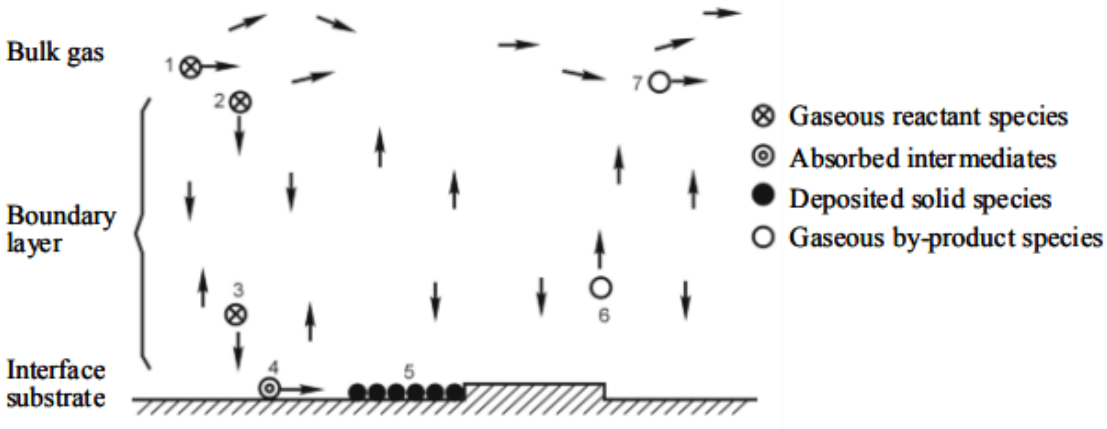

Figure 8: Schematic depiction of the seven mechanistical steps in a CVD process. Picture taken from [67]

The mechanistic steps shown in Figure 8 are [66], [67]:

1.) Flow of the reactant gases through the reaction chamber
2.) Diffusion of the reactants from the bulk gas through the boundary layer to the surface
3.) Adsorption of the reactive gases on the surface
4.) Chemical reaction between the substrate and the reactive adsorbent or the adsorbent and the gaseous phase
5.) Desorption of adsorbed molecules (by-products) from the surface
6.) Diffusion of the desorbed species through the boundary layer
7.) Unreacted gas species and gaseous by-products are forced to leave the system

4.2 Process parameters of a CVD setup

The thermodynamics and kinetics of a CVD can be defined by the temperature of the substrate or the whole vacuum chamber, pressure, gas flow and the reactant gas concentration. Due to the different chemical reactions, for instance oxidation/reduction, hydrolysis or pyrolysis, which can appear during a CVD, these process parameters have to be determined individually for each application. With the regulation of the temperature the location of the reaction can be controlled, so that the reaction occurs on the substrate and not in the gas phase. Another important process in CVD is the transportation of the reactant gas to the substrate surface and this process is defined by the reactant gas partial pressure, the total pressure in the reaction chamber and the reactor geometry. [64]

Although CVD processes can be carried out at atmospheric pressure, nowadays the most CVD processes are performed under high vacuum to reduce the pressure dependency of the deposited film properties. [64]

4.3 Types of CVD

CVD processes can be divided into different types, which differ in the way the energy for the chemical reaction is provided. The most used types of CVD methods are listed below:

- Thermally activated CVD (TACVD)
- Plasma enhanced CVD (PECVD)

Furthermore, there are many different very special types of CVD, which are used in very specific applications, for instance atomic layer epitaxy (ALE). ALE is used to grow

a monoatomic layer on a surface in a sequence. Other special CVD types are metal-organic CVD (MOCVD), where metal-organic precursors are used to form deposited films, electrochemical vapor deposition (EVP), flame assisted vapor deposition (FAVD) or photo-assisted chemical vapor deposition (PACVD). [64, 67]

In the following sections the two main types of CVD, thermally activated and plasma enhanced CVD, are described in more detail and some industrial applications are mentioned.

- **Thermally activated CVD**

To deposit coatings with thermal activated CVD, a rather high temperature between 800 °C and 2000 °C is needed, which is provided by hot plate heating, radiant heating, resistance heating or high-frequency induction. Moreover, two types of reactors can be used, which differ in the location of the heating instruments. One type is the hot-wall reactor, where the whole reactor is heated to the needed reaction temperature. The advantages of such a reactor are the variable size, so that large quantities of materials can be coated in one process step, and the precise control of the reaction conditions. However, a disadvantage is the coating of not only the substrate but every part of the reactor, which leads to depositions on the reactor walls which have to be cleaned periodically. The second reactor type is the so-called cold-wall reactor. Here, only the substrate is heated and the rest of the reactor is cooler to prevent depositions on the reactor parts, because most CVD reactions are endothermic and so they only occur on the hottest parts in the reactor. [68]

Furthermore, thermal activated CVD can be run in pressure ranges from atmospheric pressure (APCVD) to low pressure (LPCVD) and ultra-high vacuum (UHVCVD). The reduced pressure does not change the chemical reactions, it changes the rate limiting step during deposition, because at lower pressures the mass transfer rate of the reaction gas is higher than the reaction rate at the surface, which leads to more uniform depositions. [64]

The main industrial applications for thermal activated CVD are the production of amorphous and the more interesting polycrystalline silicon [69] for semiconductor industry, dielectrics for microelectronics [70] and thick ceramic coatings to protect mechanical devices [64].

- **Plasma-enhanced CVD**

Plasma-enhanced CVD is used to deposit thin films used for semiconductor films, insulation films, photoconductive films or adhesion films for various applications in semiconductor industry or for any kind of sensors at low temperatures [71].

To start the deposition of thin films at low temperatures, electron energy (plasma) is used, which is produced by supplying electrical power with high voltages and a reduced pressure to a gas. Due to the high voltage the gas breaks down and a glow-discharge plasma is produced, which consists of electrons, ions and other excited gas species. The reaction gas, which is used for the film deposition, gets ionized or dissociated by the plasma's electrons and the chemically active ions react at or nearby the heated substrate to form a thin film. [64]

Compared to TACVD, PECVD has the advantage that the deposition of the thin film is obtained at low temperatures (mainly room temperature), which are required for sensitive substrates. However, the use of a required vacuum system and a more complex CVD reactor are more expensive than the equipment for TACVD. [64] Another disadvantage due to the low temperatures is, that obtaining a pure material is very difficult. By-products and other gases cannot desorb easily at these temperatures. Therefore, mainly hydrogen is remaining as inclusion in the deposited film. [68]

Experimental Part

5 Materials and Methods

In the following chapter, all used materials and methods to hydrophobize paper sheets in the gas phase are listed. Moreover, the analytical methods to check the degree of hydrophobization and to determine the changes in paper properties are described in detail.

5.1 Paper type

The used paper type for all experiments is called UNUT, which is a unsized and untreated raw paper. This means no sizing agents are added into the bulk or the paper surface and furthermore the paper sheet is not calendered to create a smoother surface. The most important paper properties are listed in Table 1.

Table 1: Paper properties of UNUT

Area based weight [g/m²]	89.6
Filler [%]	21.25
Pigmentation [g/cm²]	0
Surface treatment	no
Roughness (Bendtsen) [ml/min]	154.9
Porosity (Hg-porosymmetry) [%]	40.95
Surface energy (dispersive) [mN/m]	26.71
Surface energy (polar) [mN/m]	36.36
Surface energy (total) [mN/m]	63.07
Tensile strength [N/m]	4096

The used paper sheets were stored in the climate room for at least 24 hours at 23 °C and 50 % humidity before they were used in the experiments. Moreover, they were stored at least for the same time at the same conditions after the gas-phase hydrophobization to ensure same conditions for the analytical methods.

5.2 Chemicals

For the gas-phase hydrophobization with ASA, commercially available *Fennosize AS 1000* from Kemira was used.

The reactants for the esterification with trifluoroacetic anhydride (TFAA)/acetic anhydride (Ac_2O) and TFAA/acetic acid (AcOH) mixtures and hexamethyldisilazane (HMDS) for the silylation were obtained from Sigma Aldrich.
The gas phase palmitoylation was done with commercially available palmitoyl chloride, which was obtained by Sigma Aldrich.

5.3 Apparatus for the hydrophobization

Two different kinds of experimental setups were used to hydrophobize the paper sheets in the gas phase. The first setup was used for all preliminary tests and for further experiments with palmitoyl chloride and ASA, whereas the second setup was used for the hydrophobization with a mixture of trifluoroacetic anhydride (TFAA) with acetic anhydride and hexamethyldisilazane (HMDS).

5.3.1 Preliminary tests

Preliminary tests were carried out to determine the ideal reaction conditions for all used sizing agents. The setup for these experiments is depicted in Figure 9 and Figure 10.

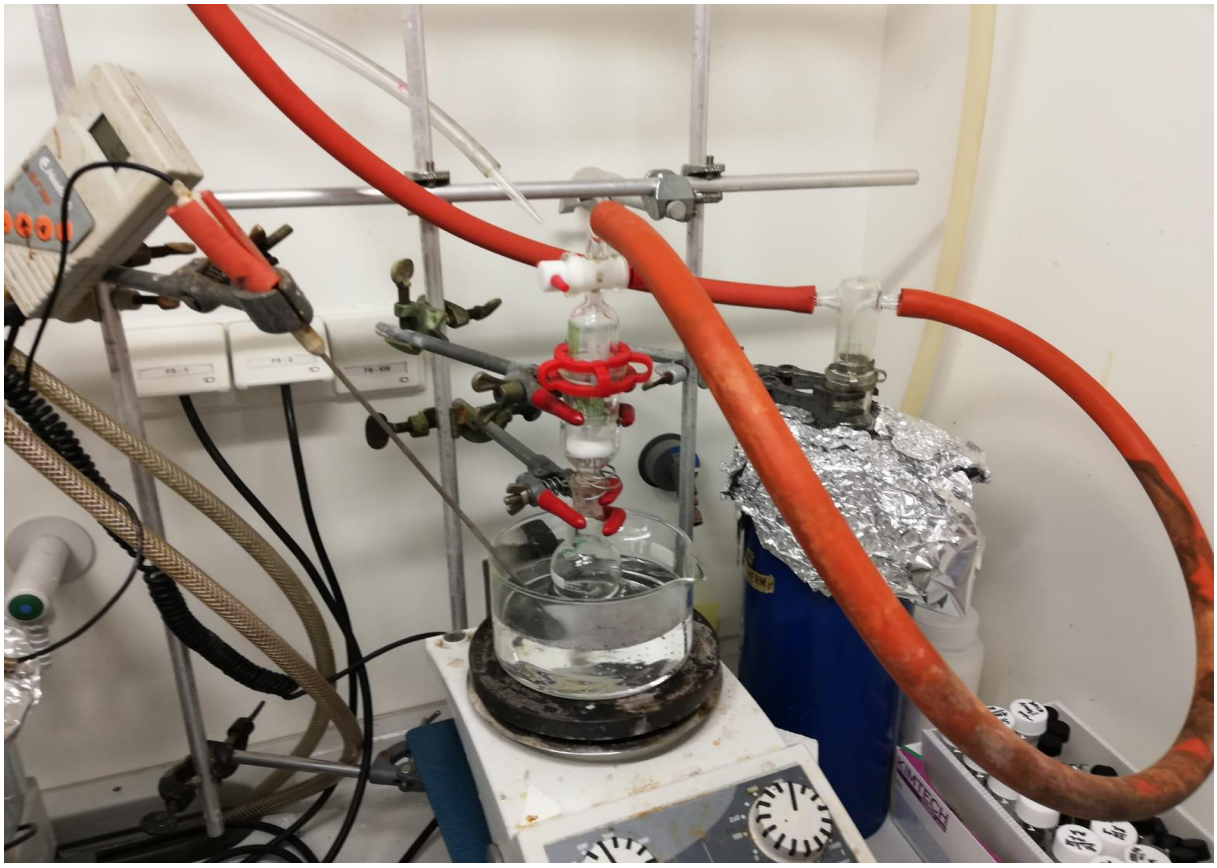

Figure 9: Experimental setup for the preliminary tests containing a cold trap, a round flask for the sizing agent, a reduction combined with an olive as reaction chamber and a water bath to heat up the sizing agent.

The setup consists of a cool trap to prevent by-products or the sizing agent to flow into the vacuum pump, a 10 ml round flask equipped with a stir bar, a reaction chamber (reduction combined with an olive) and a heating bath (water). With this setup five paper stripes with a dimension 1.5 cm x 5 cm could be hydrophobized in one pass.

Figure 10: Enlarged picture of the reaction chamber consisting of a reduction combined with an olive. A Teflon disc with little holes is used to keep the paper sheets in the right position.

5.3.2 Scaled up setup

To hydrophobize larger paper sheets in the size of A5 a desiccator was used, which was equipped with a rubber seal, an intermediate base and a glass bowl for the sizing agent. The paper sheets were fixed with a yarn on both sides and were hung up in the desiccator as seen in **Figure 11.** To reach the required temperature for the evaporation of the sizing agent, the desiccator was placed in a laboratory oven.

Figure 11: Scaled up setup to hydrophobize larger paper sheets in a desiccator. The paper sheet was hung up via a yarn and the sizing agent was placed in a glass bowl under the intermediate base.

5.4 Methods used for hydrophobization

In this chapter different methods with different sizing agents to hydrophobize paper sheets are listed.

5.4.1 CVD with ASA

The gas-phase ASA deposition was carried out with the preliminary setup at 50 and 100 °C at 20 mbar. 2 ml of the highly viscous ASA was added into the 10 ml round flask equipped with a stirring bar. Both reactions were done for two hours. The reaction occurring during the hydrophobization can be seen in Scheme 3 in Chapter 2.4.

5.4.2 Gas-phase palmitoyl chloride deposition

The gas phase hydrophobization was done with commercially available palmitoyl chloride, which was obtained by Sigma Aldrich. The preliminary setup was used at a pressure of 10 mbar, at 180 °C and for two hours. Therefore, palmitoyl chloride (2 ml, 6.6 mmol) were added into the 10 ml round flask equipped with a stirring bar. To reduce condensation of the reagent in the reaction chamber the whole chamber was wrapped with aluminum foil.

5.4.3 Gas-phase esterification with anhydride mixtures

A mixture of TFAA and Ac_2O was produced by adding Ac_2O (2 ml, 21 mmol) to TFAA (1 ml, 7.2 mmol). The same procedure was done for TFAA and AcOH. All experiments with these mixtures were carried out at 40 °C and 400 mbar and the reaction time was varied (15, 30 and 60 minutes).

The scaled-up reaction was carried out at room temperature at 400 mbar for 5 minutes with the same amount of reactants.

5.4.4 Silylation with HMDS

UNUT paper was silylated with hexamethyldisilazane, which was obtained from Sigma Aldrich.

The silylation with the small setup (Figure 9) was carried out at 100 °C and 400 mbar with varying reaction times from 15 to 60 minutes. The silylation in the desiccator (Figure 11) was carried out for 24 hours at 40 °C and 400 mbar. For this setup, HMDS (4 ml, 19 mmol) were added into a glass bowl and placed underneath the paper sheet in the desiccator. Moreover, an experiment with a mask made of aluminum foil was done to check the diffusion of the HMDS through the pore system of the paper,

depicted in Figure 12. Also, an ageing test was carried out to check the contact angle behavior over time in periods of seven days.

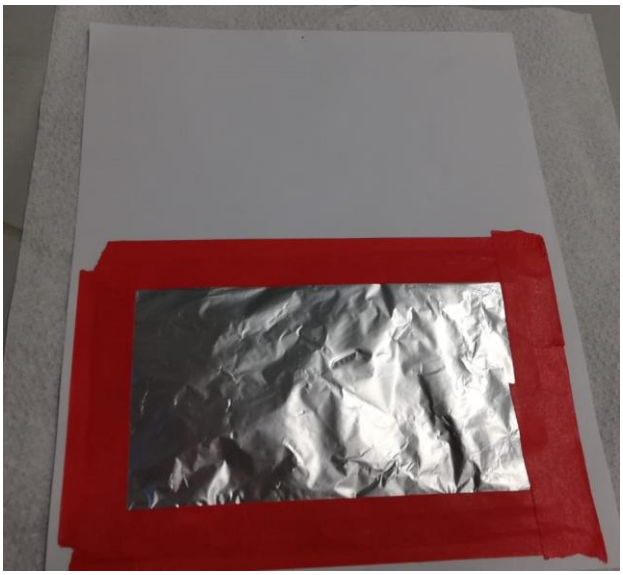

Figure 12: UNUT paper sheet with an aluminum foil mask, which is fixed with an isolating tape to prevent contact with HMDS during the deposition.

5.5 Analytical methods

In this chapter all analytical measurements to evaluate the hydrophobization degree of the modified samples are listed. Moreover, techniques to determine the impact of the modification methods on the paper properties are shown.

5.5.1 Methods to evaluate if hydrophobization was achieved

- ***Contact angle measurements***

Contact angle measurements were carried out with a Fibro DAT 1100 instrument with a drop volume of 4 µl. The used liquid was distilled H_2O. During the experiment the calculated contact angle is plotted against the time, where the change in contact angle over time is related to wetting and penetration processes. To calculate the contact angle a tangent is fitted to the outline of the interface of the drop and the paper surface. To eliminate errors the initial contact angle, which was used to compare the hydrophobization methods, was set at 200 ms, because the drop shape is changing in earlier regions due to the method of applying the drop on the paper. For the measurement, a paper stripe with a width of 15 mm is used and 10 drops were applied on the stripe during the experiment. The measurement time for one drop was set to

one minute. The contact angle measurements were carried out with all samples, which were modified with different sizing agents.

To determine the contact angle hysteresis and furthermore the receding and advancing contact angle a Krüss DSA 100 device was used. A 5 µl water drop was placed on the modified paper sheet via a syringe and the volume was increased with 1 µl/step till the contact angle did not change anymore to obtain the advancing contact angle. After reaching the advancing contact angle 0,3 µl/s were removed till the contact angle did not change anymore. At this point the receding contact angle was recorded. The contact angle hysteresis, advancing and receding contact angle were determined from the HMDS-modified sample.

The surface energy, of the HMDS-modified paper sample, was experimentally analyzed with contact angle measurements with three different test liquids using a Dataphysics OCA 200 device. The overall surface tensions (ST) and their polar and dispersive components are shown in Table 2.

Table 2: Surface tensions (ST) and their polar and dispersive component of the used test liquids to calculate the surface energy of paper sheets. [1]

	H_2O	Ethylene glycol	Diiodomethane
ST_{tot} [mN/m]	72.80	47.70	50.00
ST_{polar} [mN/m]	46.80	21.30	2.60
$ST_{dispersive}$ [mN/m]	26.00	26.40	47.40

On the sample five drops of each test liquid (V = 2 µl) were applied, and the contact angle was measured. The received data was introduced in the program SCA 20 and the surface energy and their polar and dispersive component were calculated via the OWRK method, described in Chapter 3.3.1. [54, 56]

- ***Penetration Dynamics Analyzer (PDA) – ultrasonic liquid penetration***

For all modified substrates the Emtec Penetration Analyzer 2.0 was used, and the measurement frequency was set to 2 MHz. The paper sheets were cut into rectangles of 7 cm x 5 cm and were fixed on the sample holder with a two-sided adhesive tape.

[1] Values of the surface tensions and their polar and dispersive component of the used test liquids are given by the computer program SCA 20.

The sample holder was placed in the measurement cell which was filled with distilled H_2O. On one side of the cell there is an ultrasonic emitter and on the other side is an ultrasonic receiver. The paper sample is quickly immersed in the liquid and ultrasonic waves are sent through the liquid and the sample from the emitter to the receiver. The ultrasonic intensity measured at the receiver is recorded over time. The ultrasonic waves get scattered, absorbed or reflected by the sample during liquid penetration and thus provide a measure for the solid-liquid interaction. [72] The setup is depicted in Figure 13. Three modified paper sheets of each kind were measured.

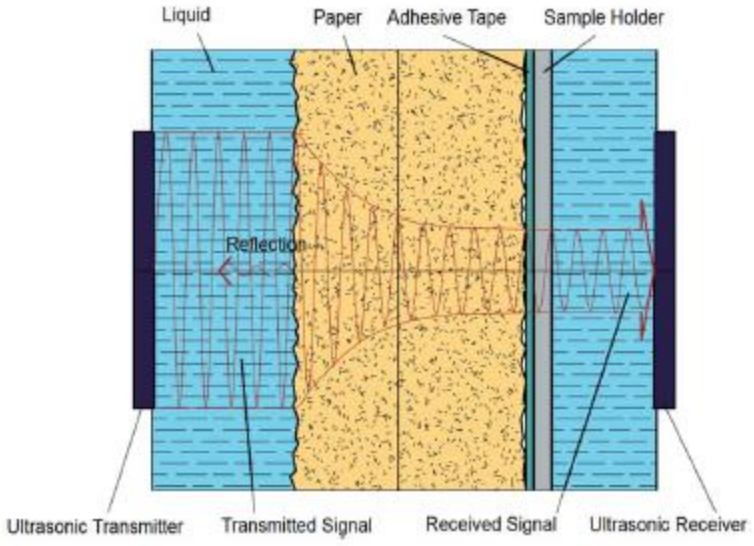

Figure 13: Experimental setup during an ultrasonic liquid penetration experiment. The red lines are representing the ultrasonic waves, which get reflected, absorbed or scattered by the sample during liquid penetration. Picture taken from [69].

- ***IR-spectroscopy***

Infrared spectra were recorded from all modified paper sheets except from the ASA-modified one, with an ALPHA FT-IR spectrometer from Bruker. The measurement was carried out with an attenuated total reflectance (ATR) attachment, with 48 scans at a resolution of 4 cm^{-1} and with a scan range between 400 and 4000 cm^{-1}. The recorded data was analyzed using OPUS 4.0 software.

- ***XPS-measurement***

An XPS-measurement was done by the Aalto University with a Kratos Ultra device to calculate the degree of substitution of the trimethylsilyl groups at the hydroxyl groups of the cellulose.

5.5.2 Methods to evaluate the impact on paper properties

- ***Mechanical tests***

The tensile tests were carried out with a FRANK tensile testing machine. The sample size was 15 mm x 140 mm and the tests were carried out in the machine direction of the paper. The clamping distance was 100 mm and the test speed was set to 20 mm/min. Three stripes of each sample were tested with this method. The tensile test was carried out for the HMDS-modified and the TFAA/Ac_2O-modified paper sheets.

- ***Roughness measurements***

The roughness of the paper samples was determined with a Bendtsen roughness tester on three individual places on one paper sheet, according to ISO 8791-2. The roughness after the hydrophobization was determined for the HMDS-modified and the TFAA/Ac_2O-modified paper sheets.

- ***Optical tests***

The optical properties of the modified paper sheets (HMDS and TFAA/Ac_2O) were analyzed by a Datacolor Elrepho spectrophotometer. The brightness was measured according to DIN ISO 11476 and the opacity according to ISO/FDIS 2471.

- ***Mercury porosimetry***

To analyze the pore structure, mercury porosimetry was carried out with an Autopore IV 9500 device. This method is based on the penetration of a non-wetting liquid (mercury) at a high pressure. The pore size is determined as a function of the pressure, which is necessary to overcome the negative capillary pressure and press the mercury into the pores. [73] The mercury porosimetry was carried out for the HMDS-modified sample.

5.5.3 Printing Tests

The printing tests were carried out with a commercially available Epson XP-342 printer equipped with an ink tank system, which is connected via hoses to the ink cartridges, as depicted in Figure 14. All printing tests were performed on the HMDS-modified and the TFAA/Ac_2O-modified paper sheets.

Figure 14: Epson printer and ink tank system for the printing tests. Picture taken from [74].

The used ink is a water-based pigment ink and the colors yellow, black, cyan and magenta were used.

In the printer settings high printing quality was chosen and furthermore the paper settings were adjusted to "Epson Matte", to ensure a high ink deposition while printing.

To analyze the smearing of the ink, a rectangular finger tester was used, equipped with a two-sided adhesive tape. On this tape a counter-paper was fixed and 10 seconds after printing the tester was pulled over the wet ink with a defined pressure. Afterwards the color density of the counter-paper was measured. The color density was measured in a square arrangement in 9 different positions (3 x 3 arrangement). Each sample was tested three times.

Additionally, color density measurements of printed cyan, yellow, black and magenta areas were carried out and the color density was measured in 9 different positions in a square 3 x 3 arrangement in the printed area. All color density measurements were carried out with a Gretag Macbeth D19 c densitometer.

Finally, printed lines and areas were investigated with an Alicona Infinite Focus Microscope (IFM) with a 50x magnification to compare feathering effects of the ink on the different paper surfaces.

6 Results

6.1 CVD with ASA

Zhang et al. [75] found out that ASA evaporates at 100 °C and they analyzed the condensate on a glass slide via infrared spectroscopy. The experimental setup can be seen in Figure 15.

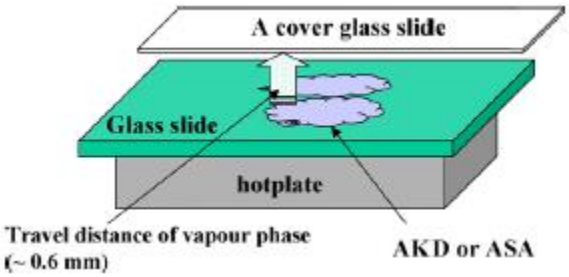

Figure 15: Experimental setup from Zhang et al. to determine the composition of ASA after evaporation and condensation. Picture taken from [75].

The analysis showed that the re-condensed ASA is the same as the originally used ASA and moreover it is free of any ASAcid, which is formed during hydrolysis and cannot be used as sizing agent [75].

As can be seen in Figure 16, the contact angle after the gas-phase ASA deposition is quite similar to the contact angle on the plain UNUT paper. Also changing the reaction temperature to 100 °C does change the contact angle in an efficient way.

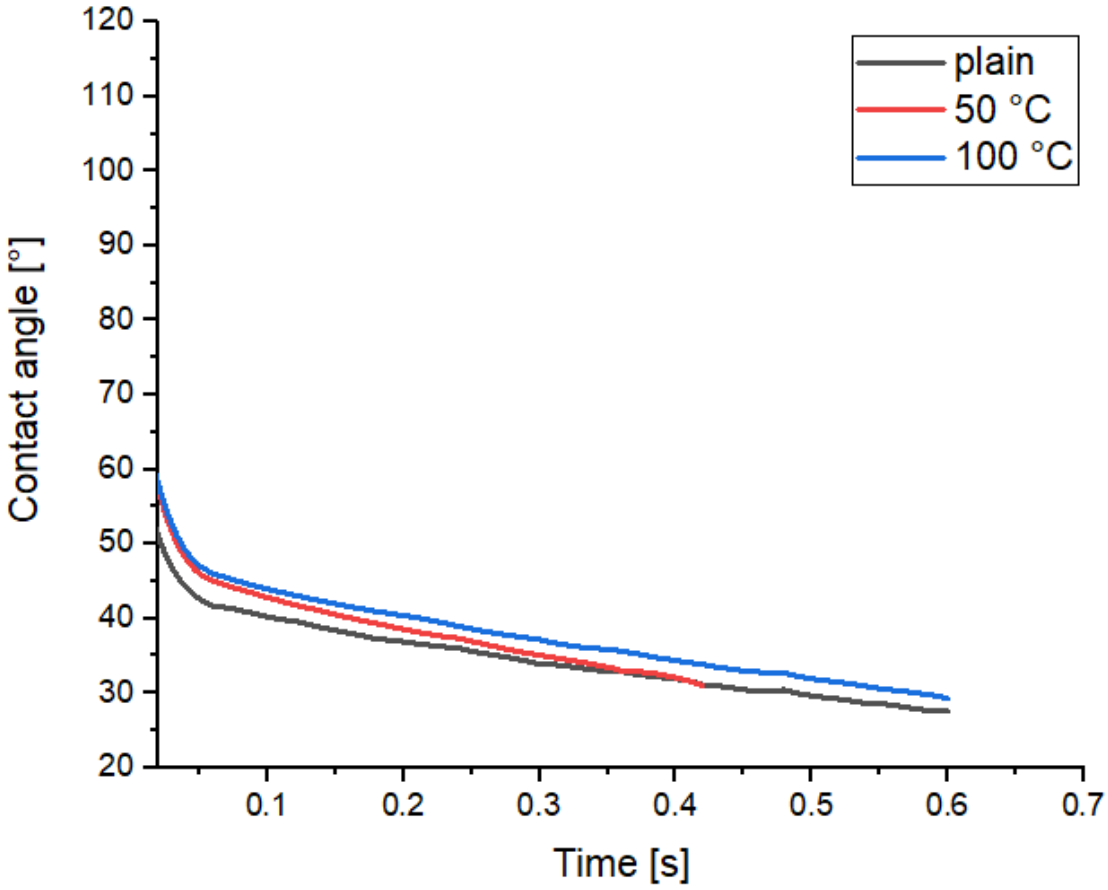

Figure 16: Contact angle measurement with 4 µl H_2O drops on an ASA-modified paper sheet over time.

Due to the poor hydrophobization and the problems of getting ASA into the gas phase, no further research was carried out on this method. Higher reaction temperatures can be an appropriate way to evaporate ASA, but higher temperatures than 100 °C can lead to a hornification of the cellulose. The hornification leads to less swelling of the fibers, lower inner surface areas and less reactivity of the cellulose [76], which would not be in line with the goal of leaving the other paper properties besides the hydrophobization unchanged.

6.2 Gas-phase palmitoyl chloride deposition

The reaction taking place while the palmitoylation with palmitoylchloride can be seen in Scheme 4.

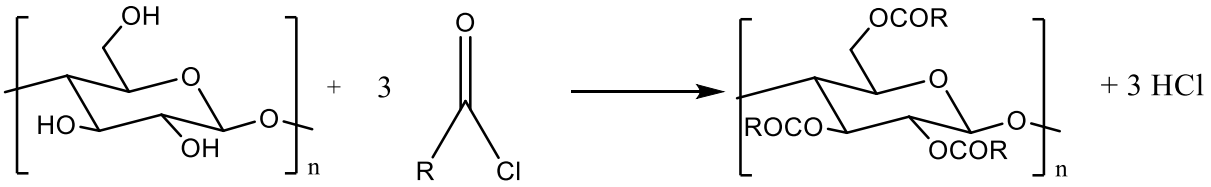

Scheme 4: Esterification of cellulose with any acyl chloride. Palmitoyl chloride R = $-CH_2(CH_2)_{13}CH_3$

As shown in Figure 17 the gas-phase palmitoylation with palmitoyl chloride worked very well at the chosen reaction conditions. However, due to the high temperature and the low pressure necessary to evaporate the palmitoyl chloride, the scale-up of the hydrophobization setup was problematic.

The contact angle at 200 ms is 117 ° ± 3 ° compared to the unmodified UNUT paper with 37 ° ± 1 °. Furthermore, the contact angle of the palmitoylated paper is stable over time and no penetration occurs over the measuring time of one minute.

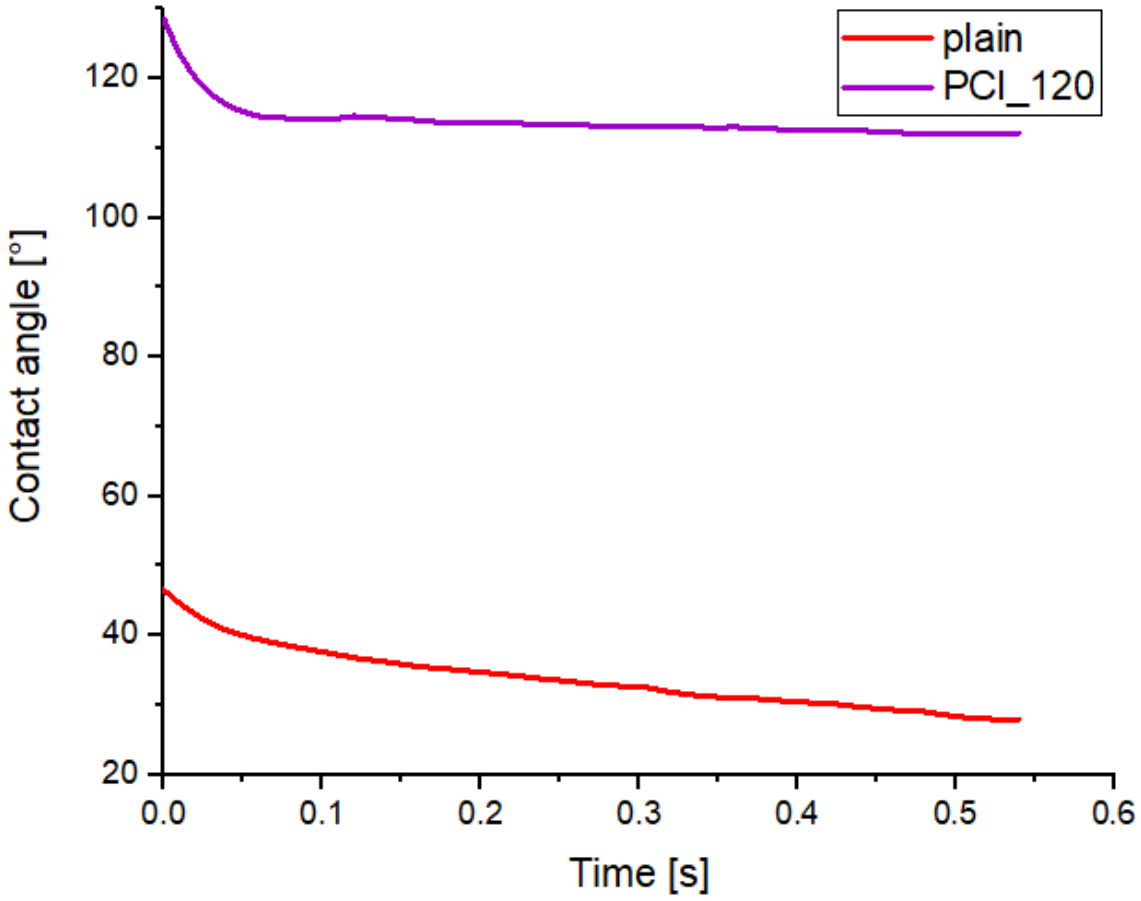

Figure 17: Contact angle measurement with 4 µl H_2O drops on a palmitoylated paper sheet over time.

In Figure 18 the comparison of the ATR-IR spectra of the plain paper and the palmitoylated paper sheet can be seen. The bands in the plain paper correspond to the bands of pulp cellulose [77]. The bands in the region of 2900 cm^{-1} to 3600 cm^{-1} are characteristic for the stretching vibration of O-H and C-H bonds and the broad band at 3330 cm^{-1} corresponds to the O-H stretching vibrations. In addition, the band at 2990 cm^{-1} corresponds to the C-H stretching vibration of hydrocarbon substituents. More characteristic bands are at 1428 cm^{-1}, 1367 cm^{-1}, 1334 cm^{-1}, 1027 cm^{-1} and 896 cm^{-1}, which are attributed to the stretching and bending vibrations of $-CH_2$, -CH, -OH and -CO bonds in cellulose. [77]

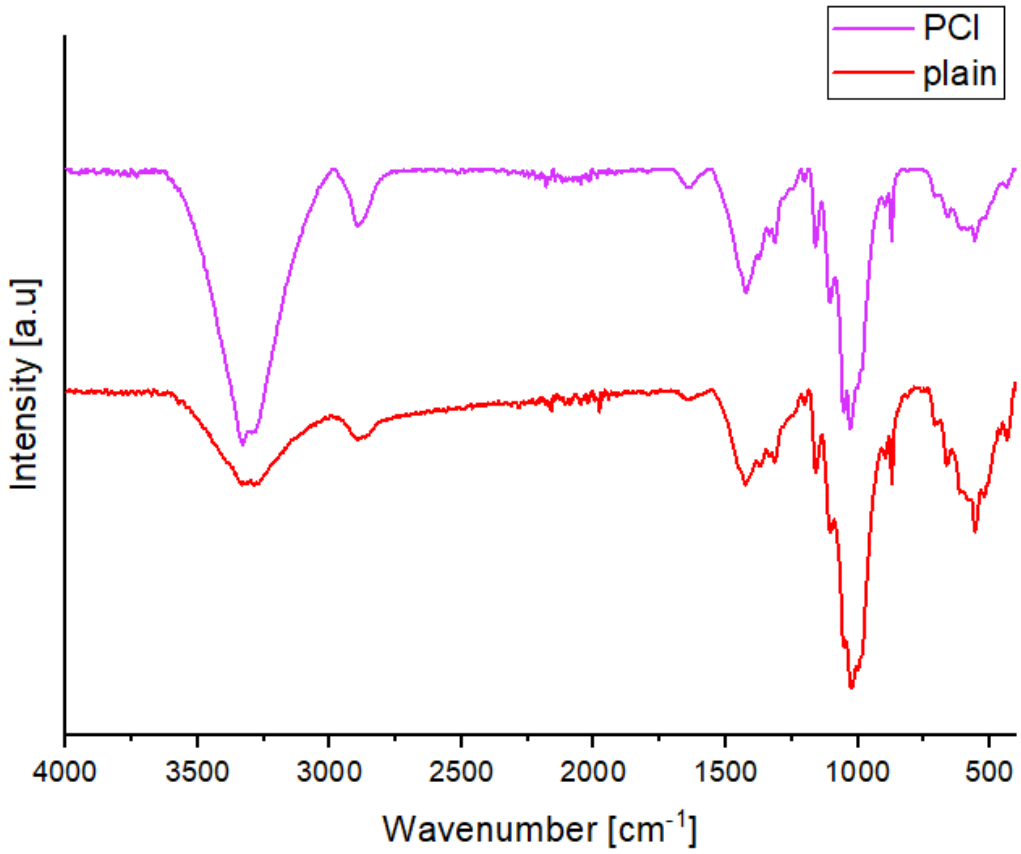

Figure 18: Comparison of the ATR-IR spectrum of the plain paper and the palmitoylated paper sheet

A closer look at the two IR-spectra reveals that the bands in both spectra do not differ from each other. Palmitoylated cellulose should have a characteristic band at 1730 cm^{-1}, which comes from the ester carboxyl bond formed during grafting [78], which is barely visible in the IR spectra of the palmitoylated paper sheet. Moreover, the hydroxyl parts in the range of 3000 cm^{-1} – 3600 cm^{-1} should have a reduced intensity, the band around 2900 cm^{-1}, which corresponds to the C-H stretching vibration, should show an increased intensity due to the sixteen carbon chain of the grafted moiety and there should be a new band at approximately 710 cm^{-1}, which corresponds to the $-CH_2$ vibration of the aliphatic chain [78]. Since no significant differences between the samples can be seen in the IR spectra, it can be assumed that there is a low degree of substitution of the palmitoyl moieties on the cellulose or a monolayer formation on the surface.

Due to the high evaporation temperature of 180 °C, the necessary pressure of 10 mbar and the related scale-up problems no further research and analytical investigations have been carried out with this method.

6.3 Gas-phase esterification with anhydride mixtures

In Figure 19 the contact angle change over time of a 4 µl water drop on an esterified paper sheet, which was modified with a mixture of TFAA and AcOH, can be seen. Due to the high acidity of the reactants, the pH value in the reaction chamber declined to 1 after 10 seconds. The contact angle change after 200 ms is not very high compared to the plain UNUT and the paper sheets show a high change in haptic, which means they feel very smooth and less stable. Because of these reasons, the decision was made to stop doing further research with this method.

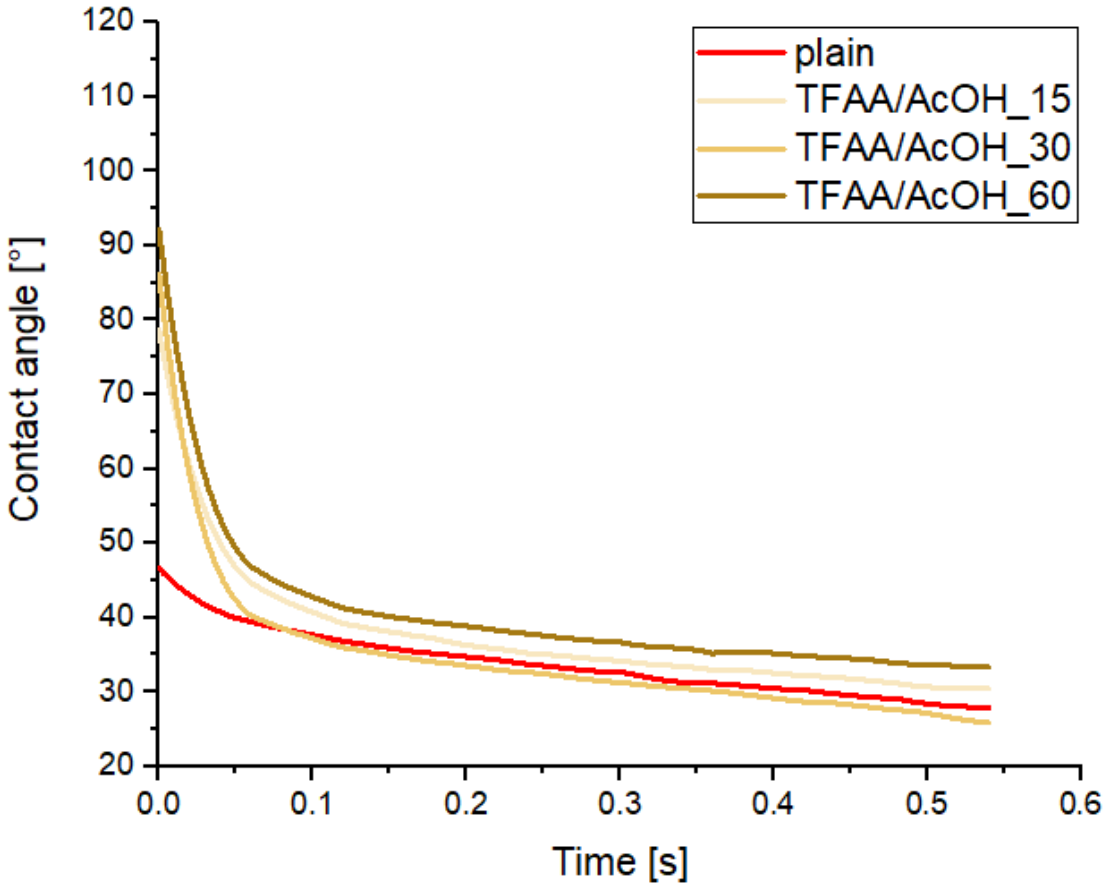

Figure 19: Contact angle measurement with 4 µl H_2O drops on an esterified paper sheet with a TFAA/AcOH mixture with different reaction times of 15, 30 and 60 minutes.

The second experiment for the gas-phase esterification with an anhydride mixture was performed with TFAA and Ac_2O. The reaction taking place can be seen in Scheme 5, where trifluoroacetyl and acetyl groups substituted the hydroxyl groups of the cellulose.

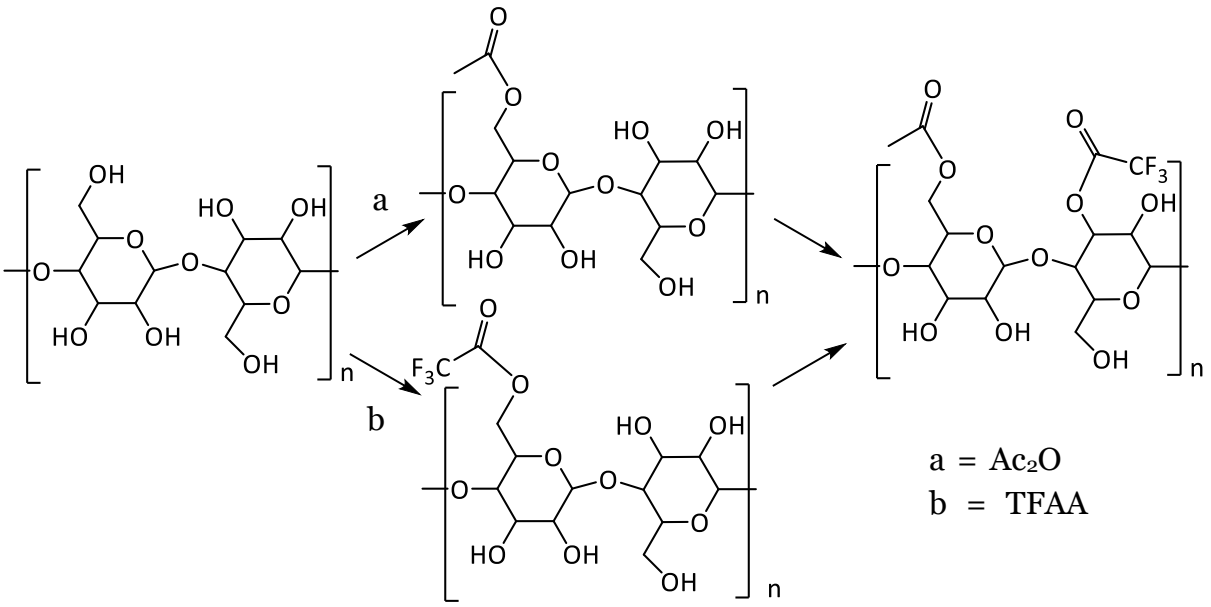

Scheme 5: Reaction of a mixture of TFAA and Ac_2O with cellulose.

The contact angle change over time after the reaction is depicted in Figure 20. The highest contact angle at 200 ms after applying the drop, 98 ° ± 3 °, was reached with a reaction time of 15 minutes. Longer reaction times resulted in lower contact angles, which was not expected.

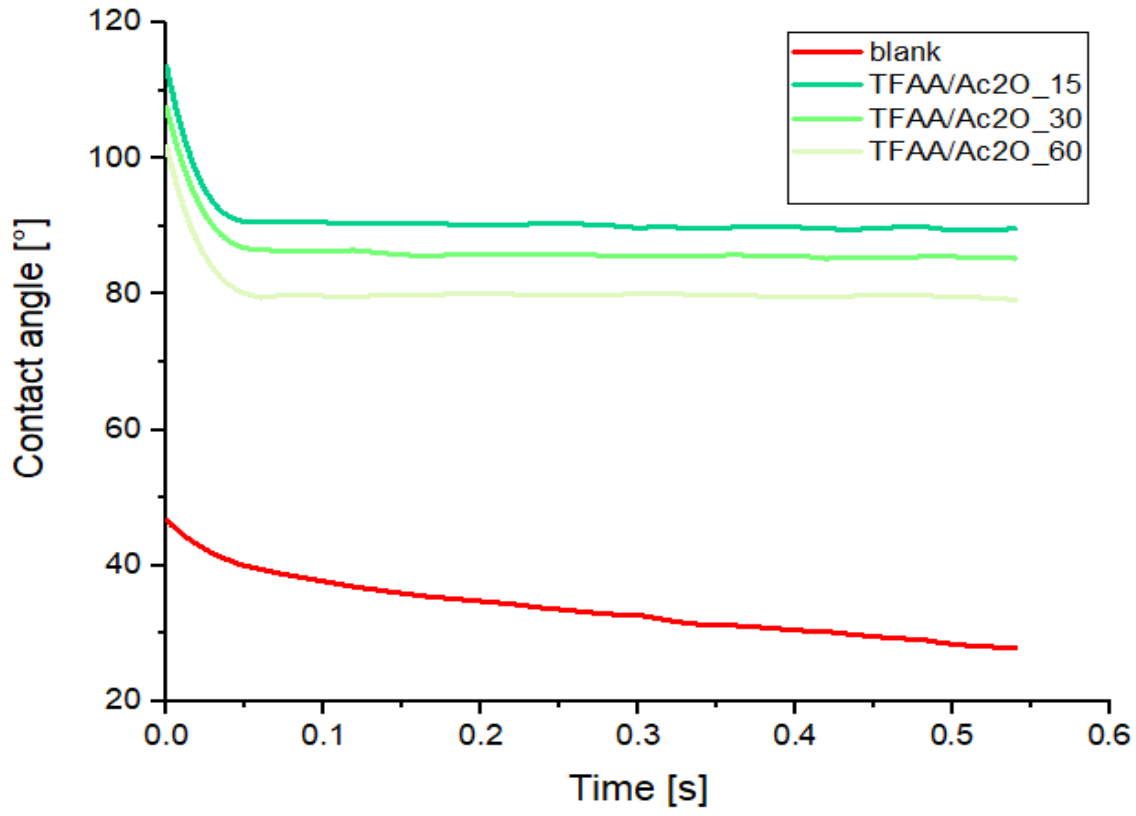

Figure 20: Contact angle measurement with 4 µl H_2O drops on an esterified paper sheet with a TFAA/Ac2O mixture with different reaction times of 15, 30 and 60 minutes.

A change of the paper appearance (degradation of the $CaCO_3$ filler) can be seen after the reaction, because the modified paper sheets have a high change in haptic and moreover the color of the sheets change from white to a greyish and greenish color, which can be seen in Figure 21. $CaCO_3$ reacts at acidic reaction conditions (formation of acetic and trifluoroacetic acid during the reaction process) under a formation of CO_2 and a calcium-salt [10], which would describe the change in optical and mechanical properties.

Figure 21: Differences in the appearance of the modified (left) and plain UNUT paper (right).

Due to the filler degradation, a compromise must be found between the degree of hydrophobization and the change of the paper properties after the reaction. Therefore, the reaction time was limited to 5 minutes and the reaction was carried out at room temperature, in order to keep the change of the paper properties as small as possible with the highest possible degree of hydrophobization. The contact angle change over time, with adapted reaction conditions, is depicted in Figure 22.

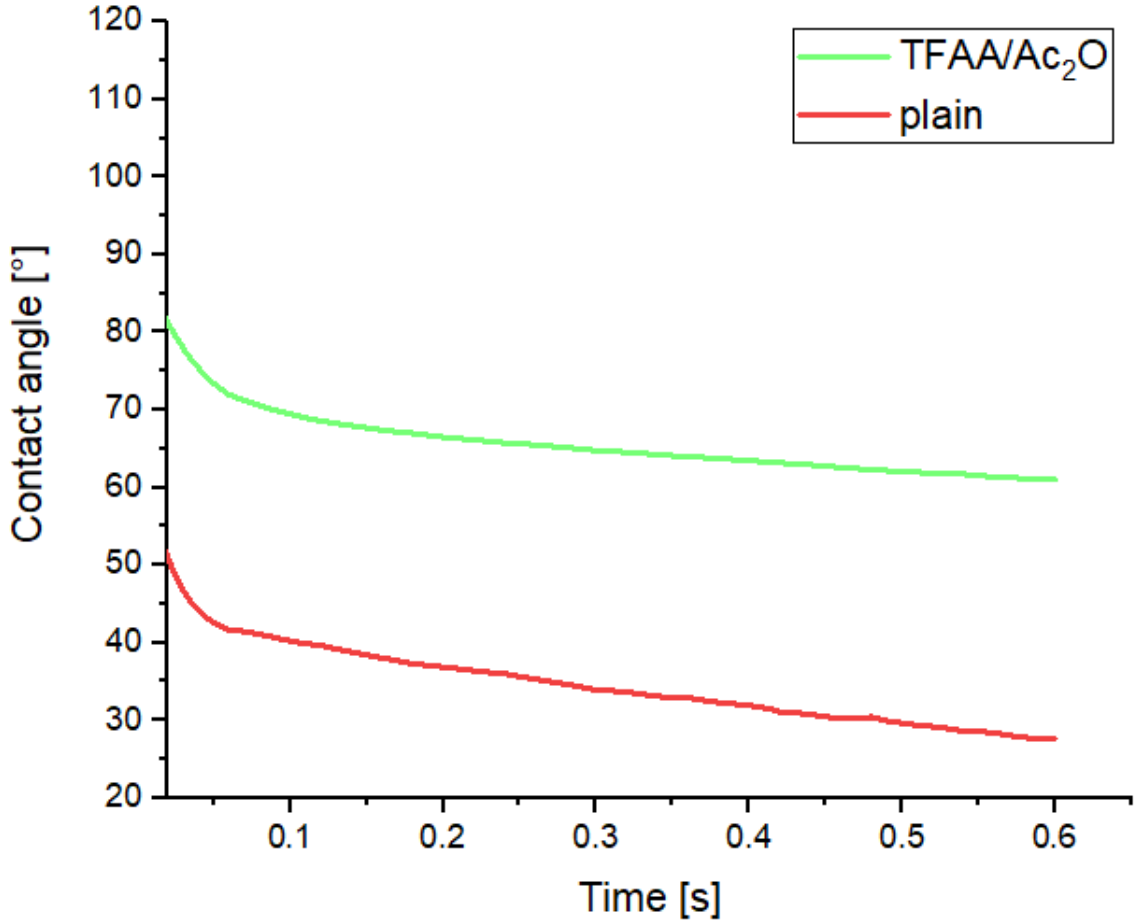

Figure 22: Contact angle measurement with 4 µl H_2O drops on an esterified paper sheet with a TFAA/Ac2O mixture after adapting the reaction conditions.

Compared to the contacts angles at 200 ms in the preliminary test, the contact angle with adapted reaction conditions was reduced by 22 ° to 76 ° ± 3°. However, there are no more visible changes in the appearance of the samples but slight changes in haptic. To analyze the changes in haptic a Bendtsen roughness test and a tensile test were made. The results can be seen in Figure 23 and Figure 24.

As shown in Figure 23 the roughness of the modified paper sheet increased from 163 ml/min ± 13 ml/min to 639 ml/min ± 52 ml/min. The very high increase of the roughness after the reaction may be due to the very acidic reaction conditions, the following destruction of the paper matrix and the loss of the filler.

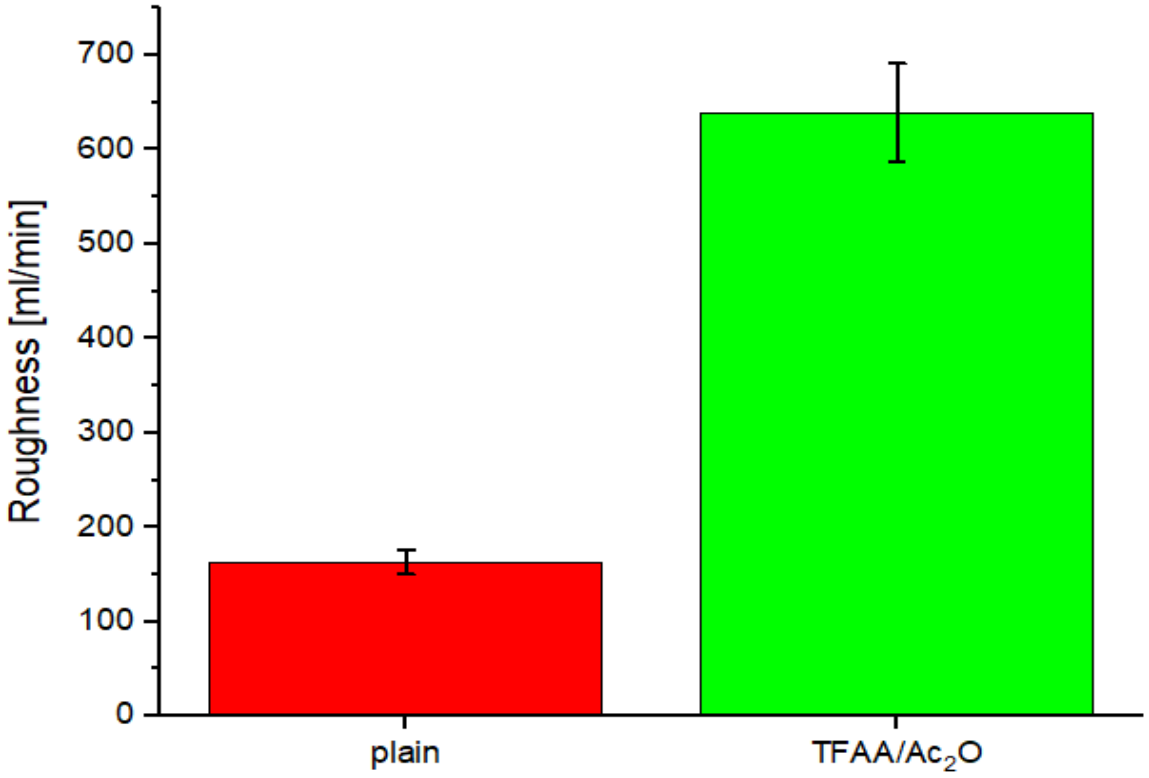

Figure 23: Bendtsen roughness test of the blank UNUT and esterified sample with TFAA/Ac_2O.

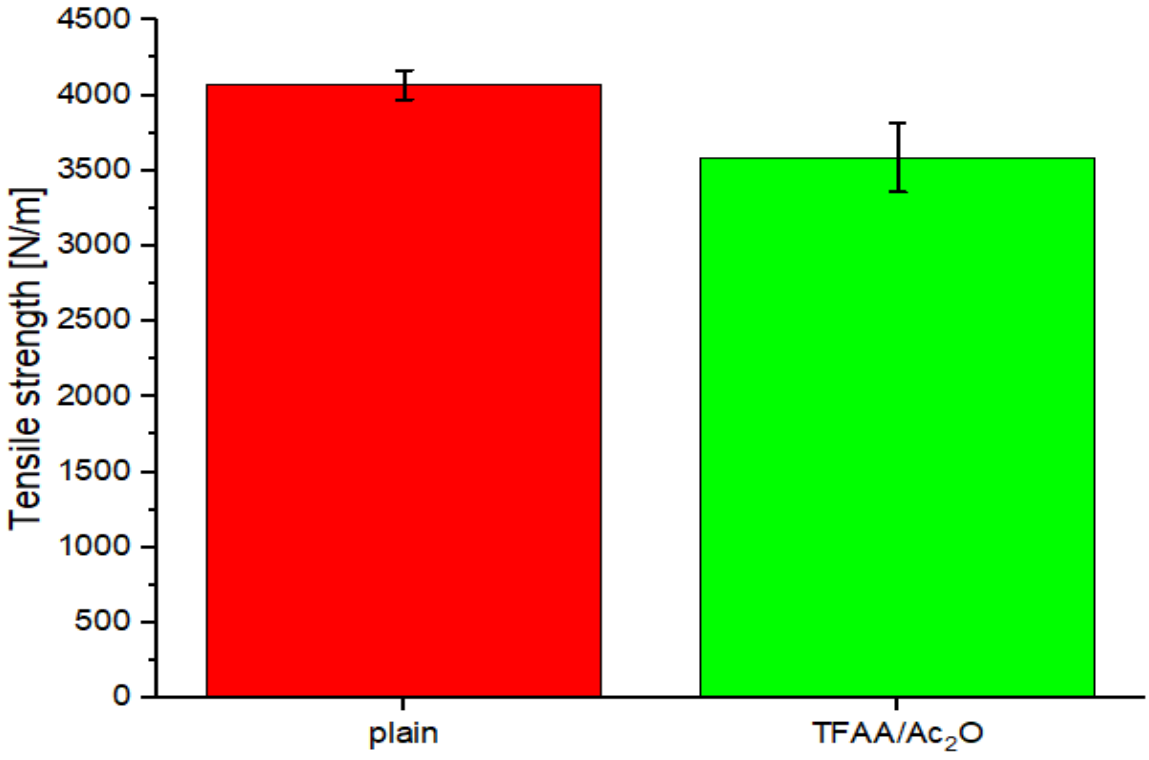

Figure 24: Tensile strength of the blank UNUT and esterified sample with TFAA/Ac_2O.

Furthermore, the tensile strength of the esterified paper sheet (Figure 24) decreased from 4069 N/m ± 97 N/m to 3586 N/m ± 230 N/m. This effect may be due to the acidic reaction conditions, where the filler was degraded.

In addition, the optical properties, opacity and brightness were measured with a photospectrometer. The opacity amounts to 95.01 % ± 0.04 % compared to the plain UNUT with 96.84 % ± 0.11 % and the brightness amounts to 98.66 % ± 0.14 % compared to 99.26 % ± 0.06 %. Both tested optical properties are nearly the same compared to the plain UNUT paper. Thus, it can be assumed, that no changes in the optical properties take place after the reaction was carried out.

Finally, an ATR-IR spectrum was recorded, which can be seen in Figure 25.

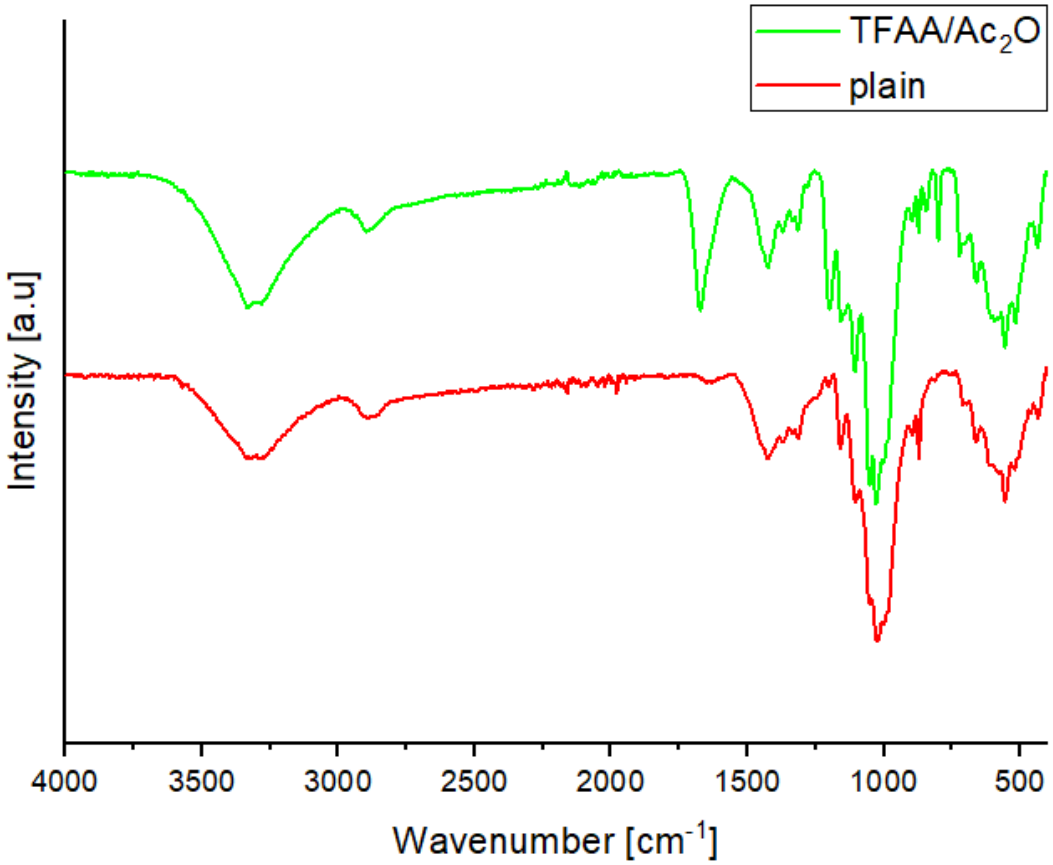

Figure 25: ATR-IR spectra of the esterified paper sample and the plain UNUT paper.

The bands of the plain paper sample are described in detail in Chapter 6.2. Comparing the IR-spectrum of the sample with the reference UNUT paper many differences can be found. The band at 1673 cm^{-1} is characteristic for the stretching vibration of the carboxyl group (C=O) of the ester bond. The band at 1200 cm^{-1} corresponds to the -FCF_2 vibrations and the band at 1160 cm^{-1} to the -FCF vibrations [79]. Furthermore, many new bands are occurring in the fingerprint region of the spectra, which is below 850 cm^{-1}, and they belong to other fluorine moieties [79].

6.4 Silylation with HMDS

Due to the small contact angle changes in the preliminary tests, which can be seen in Figure 26, the reaction time was extended in the scale-up tests. In line with earlier investigations of gas-phase hydrophobization of bleached and unbleached microfibrillated cellulose (MFC) done by Chinga-Carrasco et al. in 2012 [80], the reaction time was extended to 24 hours. The reaction occurring during the silylation of the paper sheet can be seen in Scheme 6.

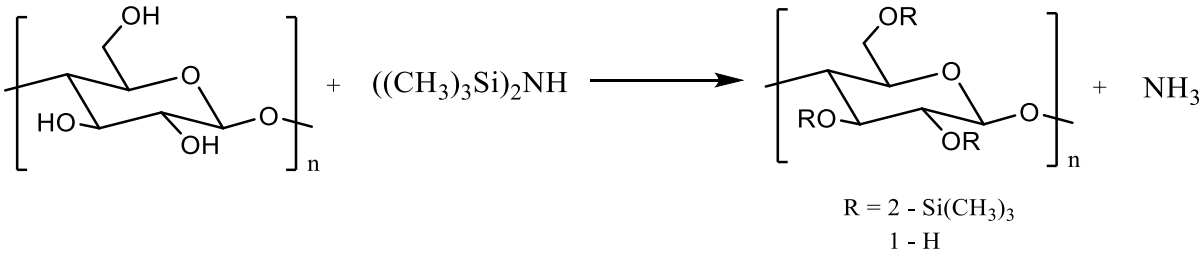

Scheme 6: Gas-phase silylation of cellulose with HMDS

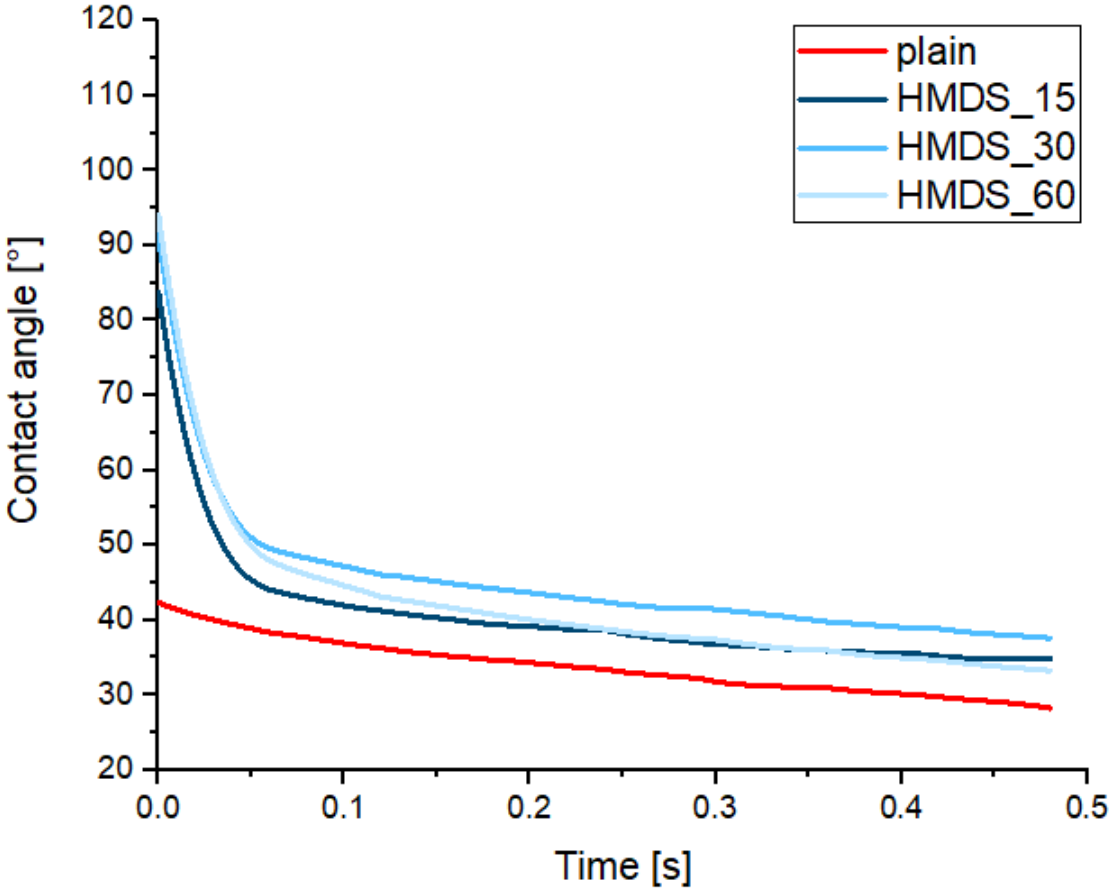

Figure 26: Contact angle measurement with 4 µl H_2O drops on a silylated paper sheet with HMDS with different reaction times of 15, 30 and 60 minutes.

It is still not clear why the contact angle is higher after 30 minutes than after 60 minutes. Nevertheless, the differences in the contact angle at 200 ms are in a range of 5° and may be attributed to measuring inaccuracies with the Fibro DAT device.

After extending the reaction time to 24 hours the contact angle at 200 ms amounts to 106 ° ± 3° and the contact angle change over time can be seen in Figure 27.

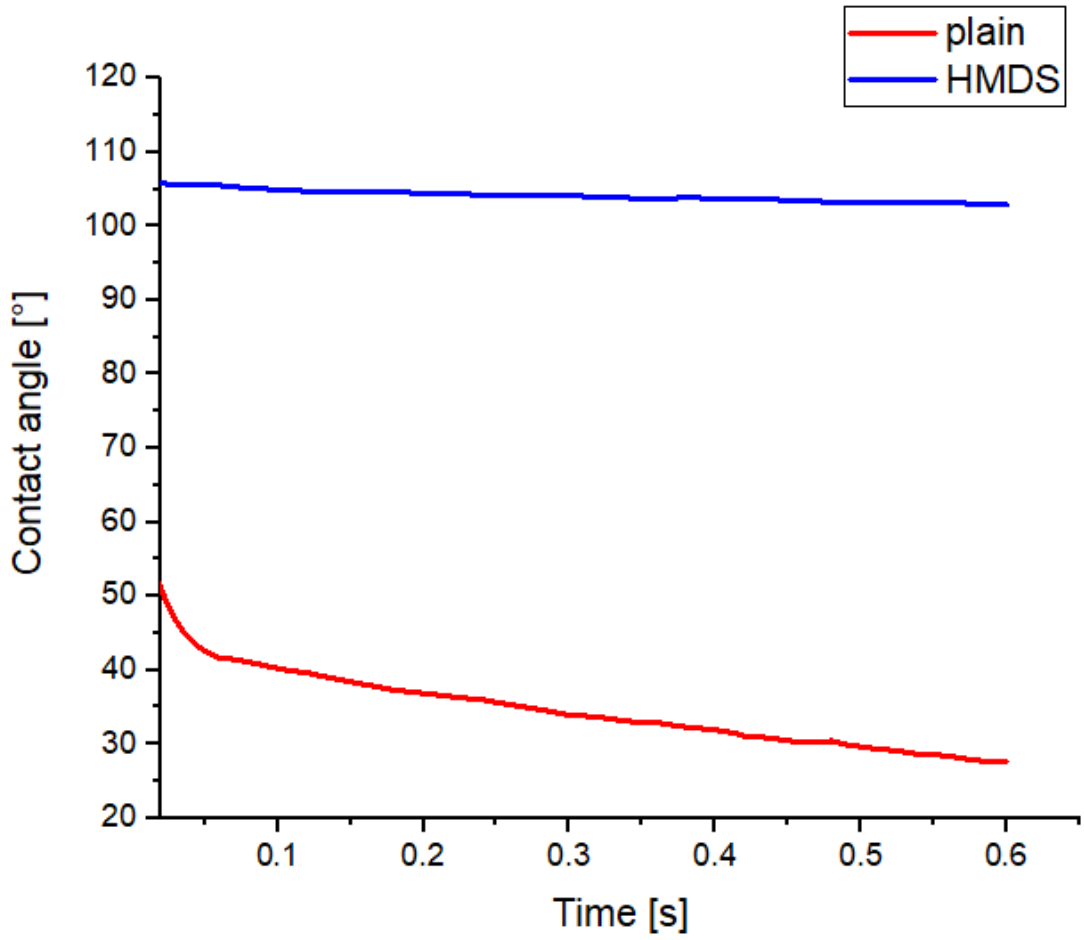

Figure 27: Contact angle measurement with 4 µl H_2O drops on a silylated paper sheet over time, after a reaction time of 24 hours.

Due to the high contact angle ($\theta > 90$ °) and furthermore the lower surface energy, no penetration of the water drops can be seen on the silylated paper sample. The applied drops are depicted in Figure 28.

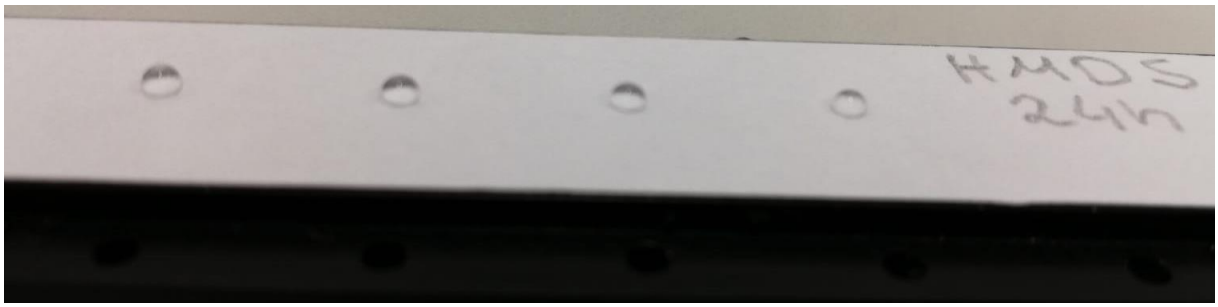

Figure 28: Applied water drops on a silylated paper sheet after the contact angle measurement.

The lack of penetration is also visible in Figure 27, because the contact angle change over time is very small, which indicates that the water cannot wet the hydrophobized surface as described in Chapter 3.

To investigate if the hydrophobization takes place not only on the paper surface but also in the bulk, an aluminum foil was fixed on both sides of the paper with an isolating tape, as depicted in Figure 12. The contact angle was then measured under the mask and beside the mask. The corresponding contact angles over time can be seen in Figure 29.

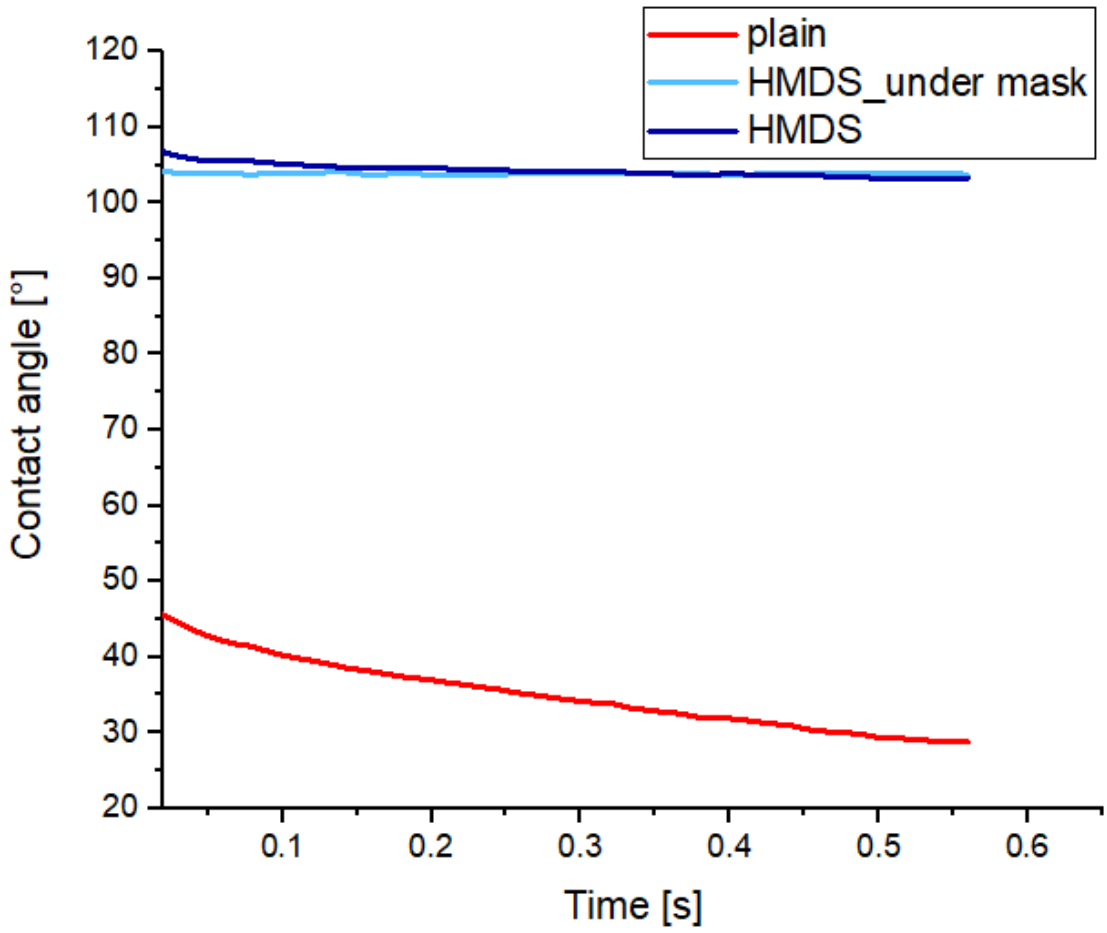

Figure 29: Comparison of the contact angles over time of the area under the aluminum mask and beside the mask, after a reaction time of 24 hours.

Since the same contact angle was measured under the mask and beside the mask it could be concluded, that the evaporated HMDS diffuses through the pore system of the paper and every fiber gets hydrophobized on the fiber surface throughout the paper sheet.

The stability of the hydrophobization was tested with an ageing test, which can be seen in Figure 30. The initial contact angles of the sample do not differ from each other, no matter whether the contact angle was measured immediately after the hydrophobization or three weeks later. The most significant differences can be seen after 14 and 21 days after the experiment was carried out, because there the slope of the contact angle curve over time is steeper. This may be due to desorption processes of adsorbed HMDS molecules, which only become noticeable after a long storage period. Nevertheless, for high-speed inkjet printing only the first 100 ms, which are called high-speed inkjet relevant time, are important and in this region the contact angle is rather stable over a period of three weeks.

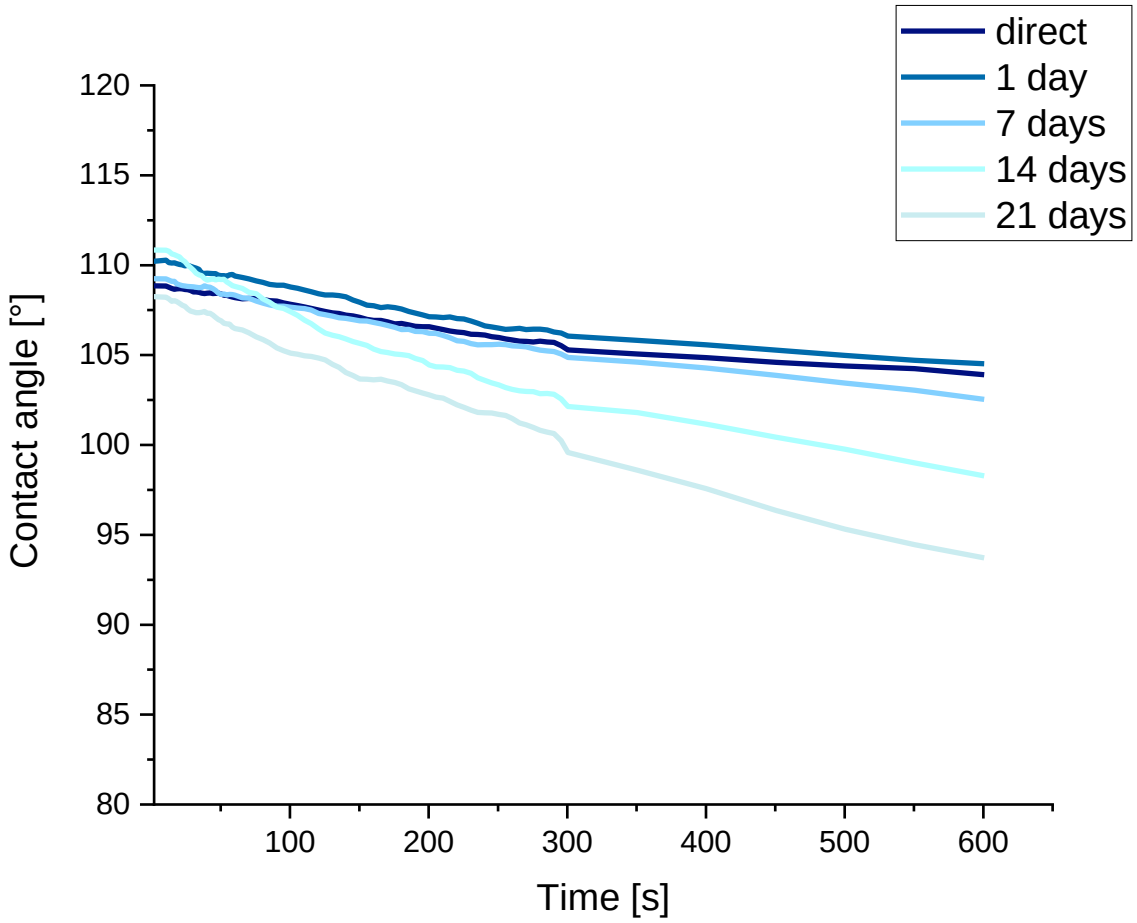

Figure 30: Ageing test of the silylated paper sheet with contact angle measurements over time at intervals of 7 days after the experiment was carried out.

In addition to the contact angle measurements over time, the contact angle hysteresis (advancing θ_{adv} and receding θ_{rec} contact angle) was investigated. The contact angles and different steps during the measurements are depicted in Figure 31. The determination of θ_{adv} and θ_{rec} was very hard because of the high roughness of paper sheets. At a certain drop size (after 6 µl were added) the contact angle became smaller again, because the shape of the drop changed due to the high paper roughness. Moreover, a faster decrease in the contact angle can be seen after measurement point 17, because the drop shape changed. Θ_{adv} was determined from the mean of the three highest measured contact angles and amounts to 131 ° ± 1 ° and θ_{red} was determined out of three points shortly before the drop shape changed and amounts to 93 ° ± 1 °. The mean of Θ_{adv} and θ_{red} is called the static contact angle θ_{stat} and it amounts to 112 ° ± 1 °.

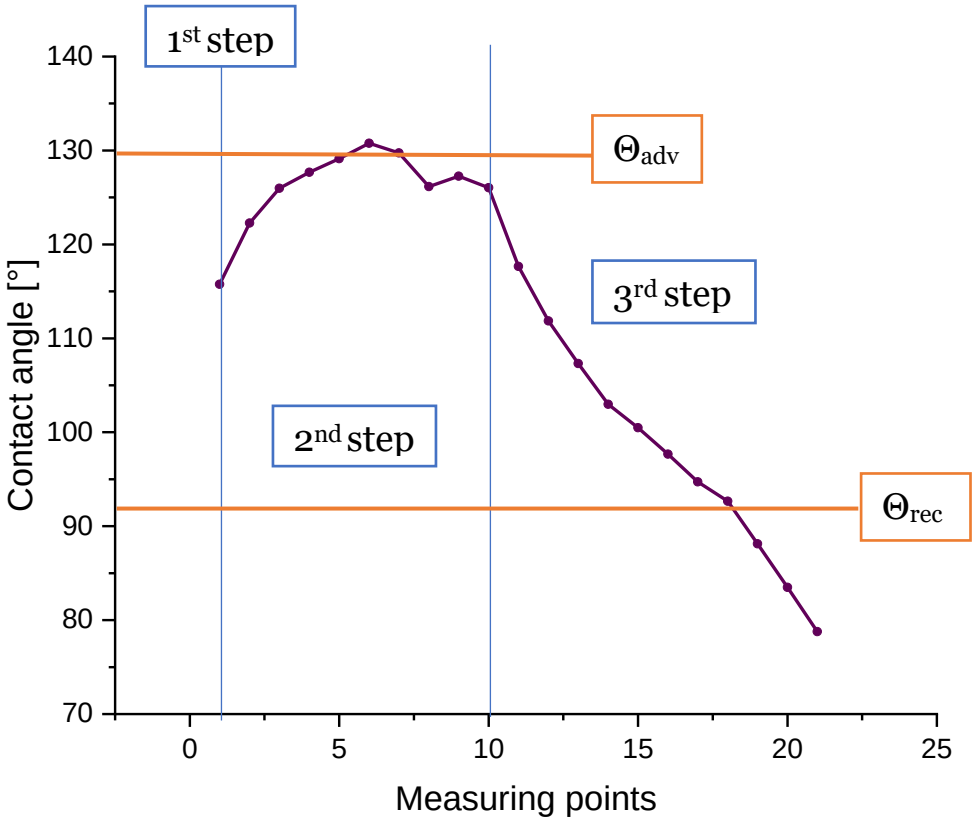

Figure 31: Measurement of the advancing θ_{adv} and receding θ_{rec} contact angle with a water drop on a silylated paper sheet.

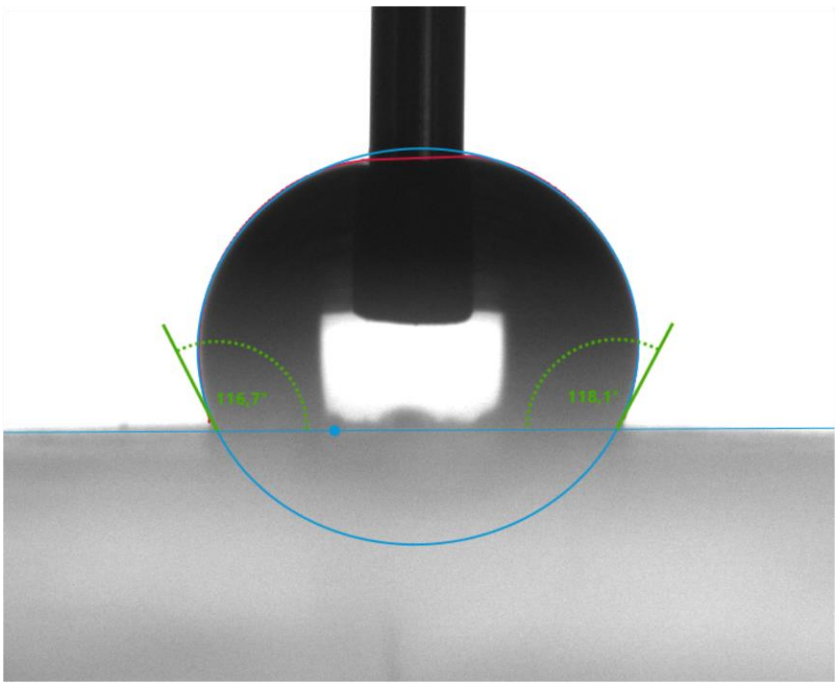

Figure 32: Initial contact angle with a 5 µl H_2O drop placed on the surface of the HMDS-modified paper.

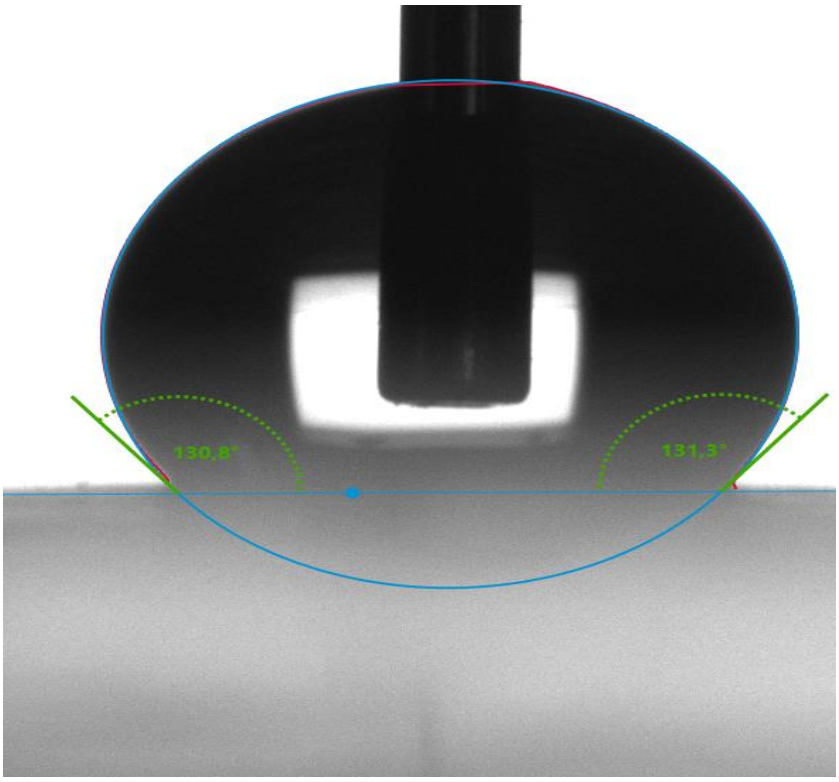

Figure 33: Advancing contact angle θ_{adv} on the surface of the HMDS-modified paper, after an addition of 6 µl H_2O through the needle of the syringe.

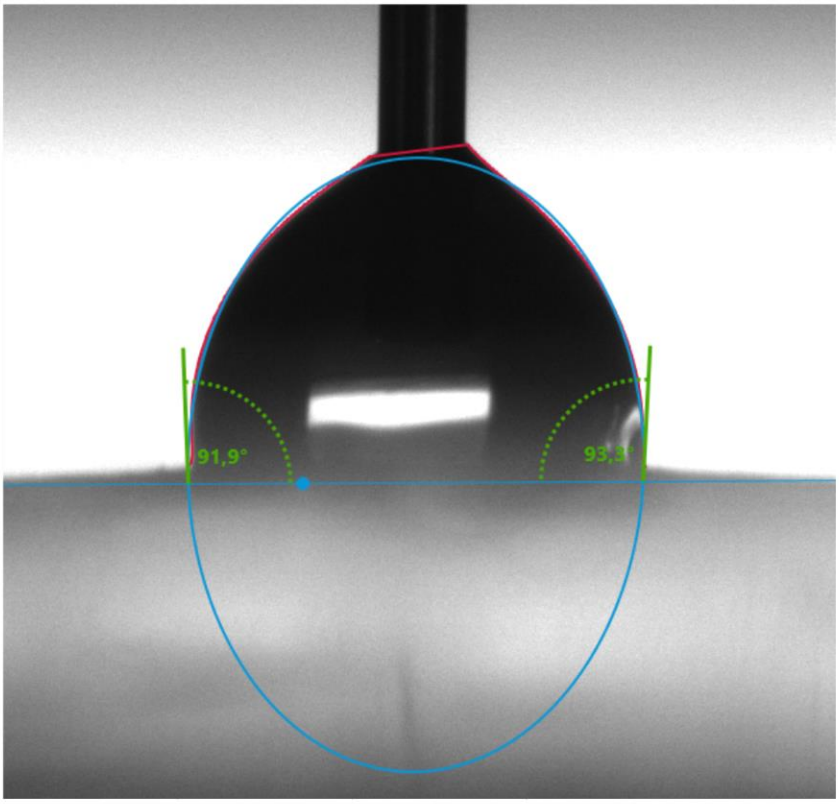

Figure 34: Receding contact angle θ_{rec} on the surface of the HMDS-modified paper, after removing H_2O from the drop, till the contact angle does not change anymore.

As expected, also the surface energy of the HMDS-modified paper is lower than of the plain UNUT paper. The total surface energy amounts to 48.91 mN/m with a polar component of 0.13 mN/m and a dispersive component of 48.78 mN/m compared to a total surface energy of the plain UNUT paper of 63.07 mN/m with a polar component of 36.36 mN/m and a dispersive one of 26.71 mN/m.

The biggest advantage of silylated paper sheets is the fact that a high degree of hydrophobization can be reached without changing the pore system or in other words the porosity during the gas-phase hydrophobization. This is shown in Figure 35, where the incremental specific intrusion of mercury is plotted against the pore diameters of the paper network. From the intrusion of mercury, the porosity of the paper samples can be calculated. The calculated porosity of the plain UNUT paper amounts to 40.95 % and the porosity of the HMDS-modified paper amounts to 44.10 %.

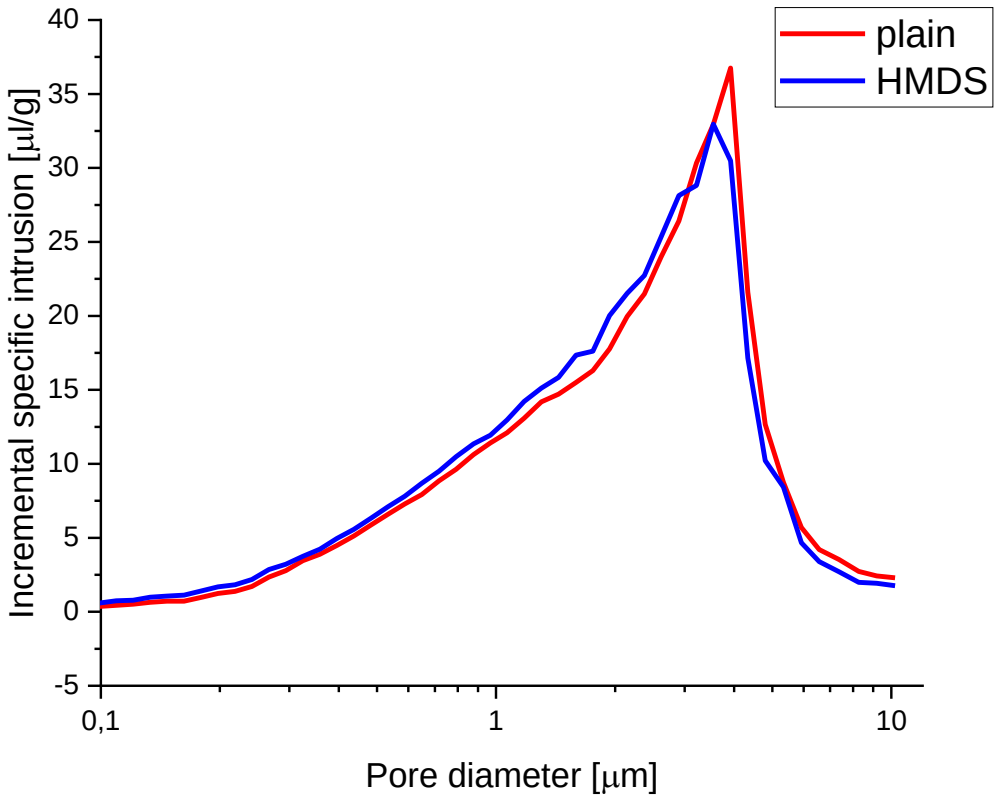

Figure 35: Hg-porosimetry measurement of the plain paper in comparison to the HMDS-modified one.

Furthermore, the tensile strength does not change during the gas-phase modification with HMDS, which can be seen in Figure 36 and also the slight change in roughness is not significant (Figure 37). The tensile strength of the modified paper sheet amounts

to 4037 N/m ± 58 N/m compared to 4069 N/m ± 13 N/m of the plain UNUT sheet. The roughness amounts to 155 ml/min ± 7 ml/min compared to 163 ml/min ± 13 ml/min. Since the mechanical properties of the modified paper sheet are not changed, it can be assumed that the paper matrix will not be significantly altered during the modification.

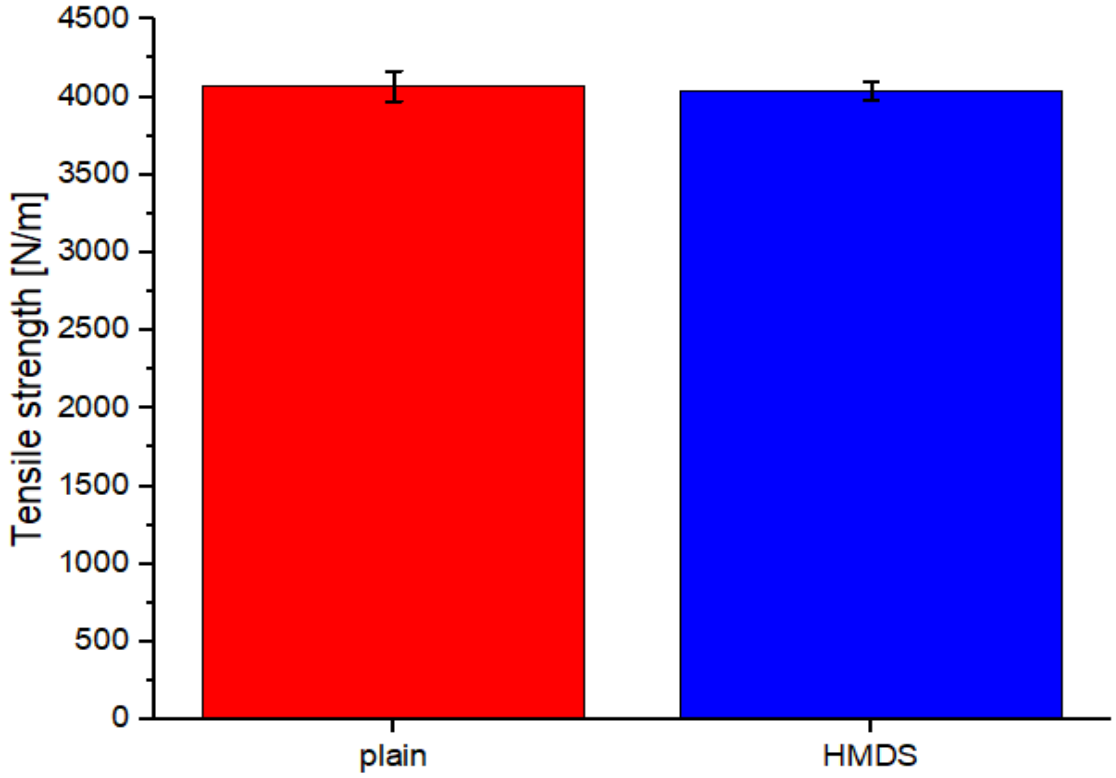

Figure 36: Tensile strength of the silylated and blank UNUT paper sheet.

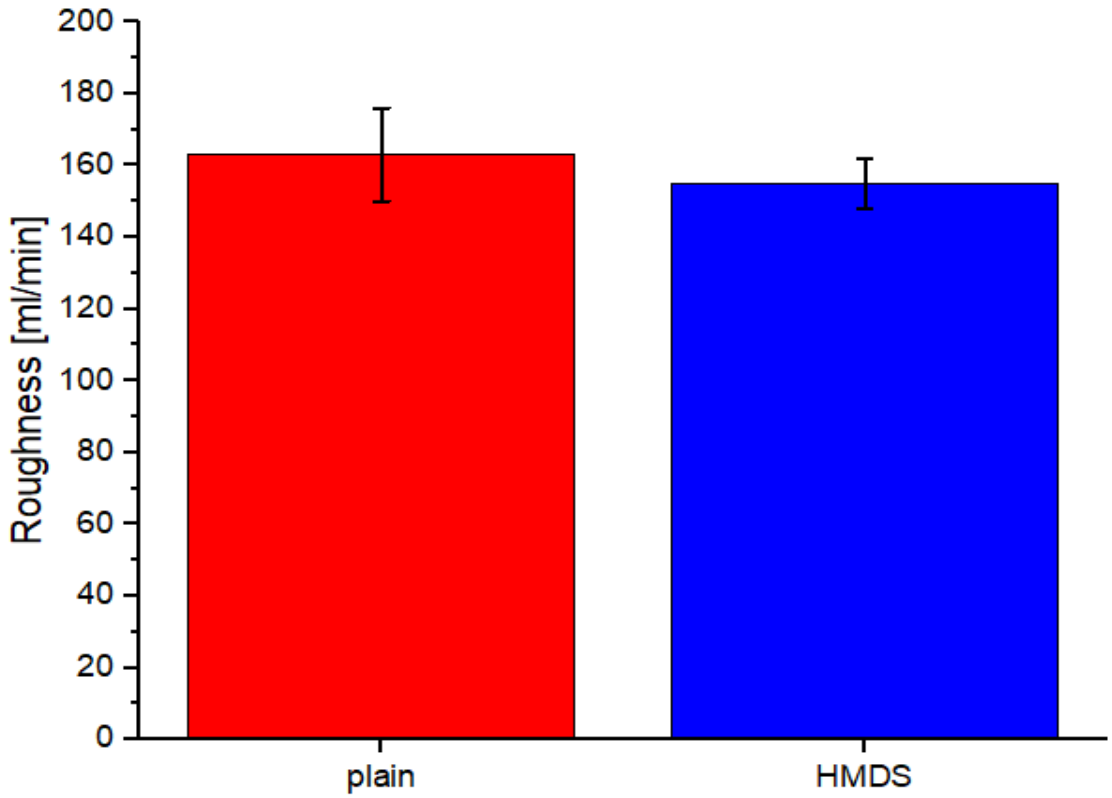

Figure 37: Measured roughness of the HMDS-modified and plain UNUT paper sheet.

In addition to the mechanical properties, the optical properties remain unchanged. The brightness was 99.31 % ± 0.04 % compared to 99.26 % ± 0.06 % of the plain UNUT paper and the opacity was 96.93 % ± 0.09 % compared to 96.84 ± 0.11 %.

Due to the surface analysis via ATR-IR measurements it could be concluded, that only a monolayer of trimethylsilyl gropus is grafted on the fiber surfaces, because no changes of the IR-spectrum after the modification are visible. The corresponding ATR-IR spectrum (Figure 38) and the bands of the plain paper sample are described in detail in Chapter 6.2. Moreover, the degree of substitution must be small, because the intensity of the -OH vibration (3000 cm^{-1} – 3600 cm^{-1}) should decrease with an increasing degree of silylation. The typical C-Si rocking vibrations at 757 cm^{-1}, 848 cm^{-1} and 1252 cm^{-1} [81] are not clearly visible because of an overlapping with the bands of the plain UNUT sheet.

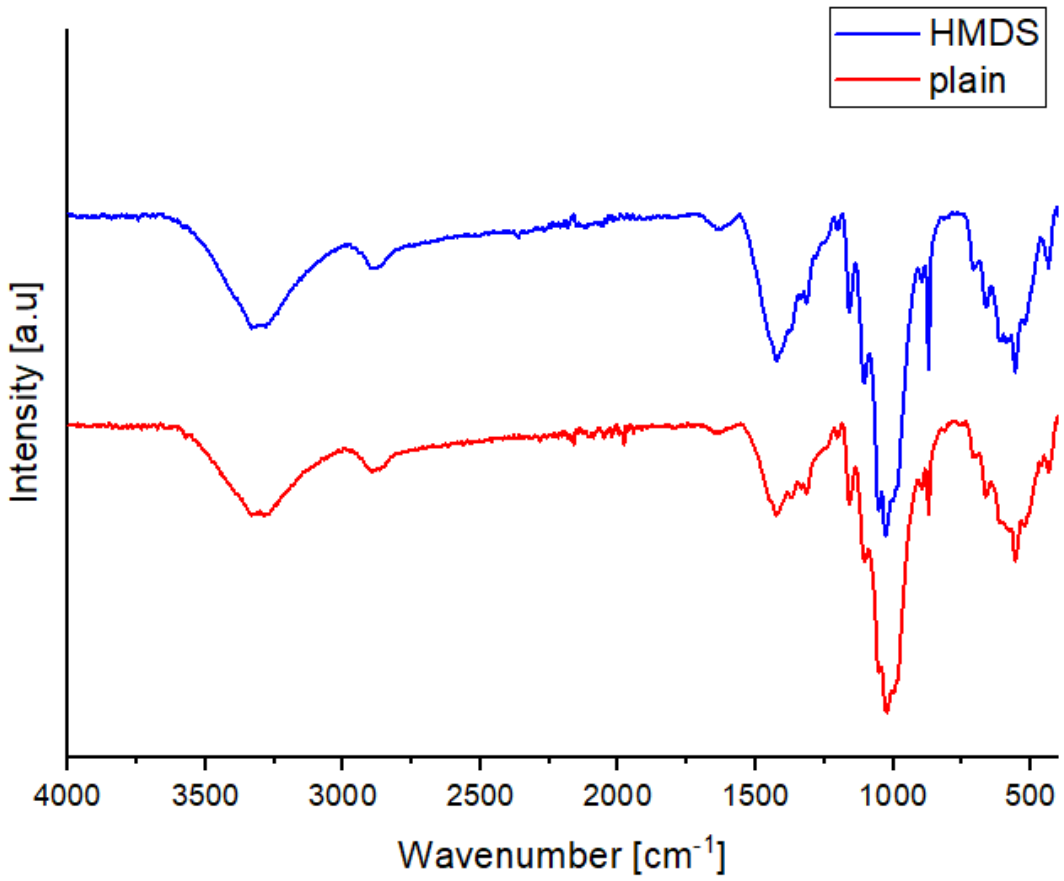

Figure 38: ATR-IR spectrum of the HMDS-modified paper sheet in comparison to a plain UNUT paper.

An XPS measurement (Figure 39) did show the presence of additional contributions in the C1s (287 eV), O1s (533 eV) and Si2p (101 eV) region stemming from trimethylsilyl groups.

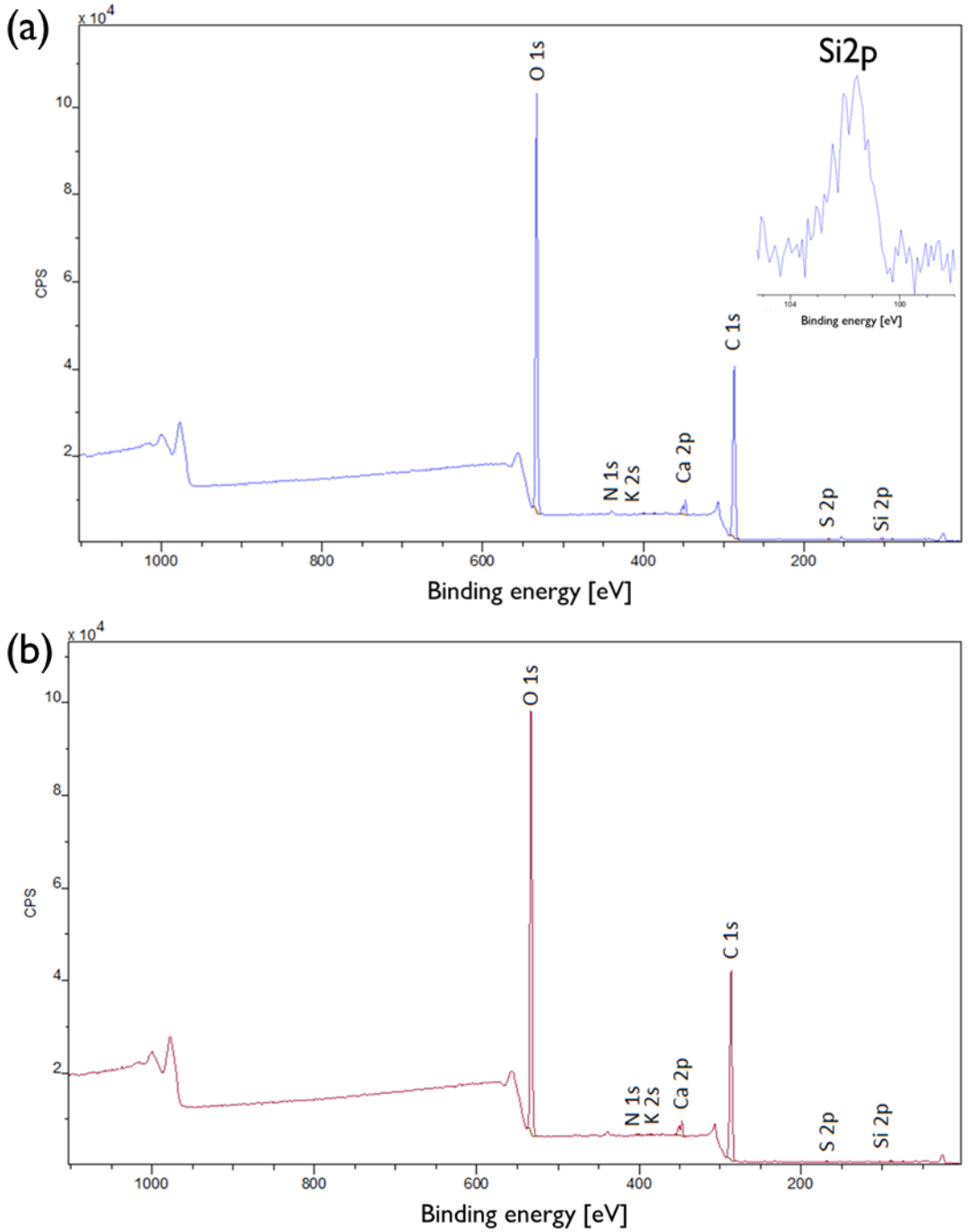

Figure 39: XPS spectra of the silylated paper sheet (a) and the untreated UNUT paper sheet (b).

The low degree of substitution was also confirmed by the amount of silica in the paper, which was used to determine an average degree of substitution. The silicon content in atomic percent on the paper surface increased from 0.16 % ± 0.05 % on the plain UNUT sheet to 0.93 % ± 0.05 % after the gas-phase hydrophobization. The atomic percentages of the elements found on the paper surface are shown in Table 3. The

DS_{TMS} was 0.1, which equals to one trimethylsilyl group on every 30th anhydroglucose unit, which is very low for a hydrophobized surface.

Table 3: Atomic percentages of the elements found on the paper surfaces.

	C_{1s} [%]	O_{1s} [%]	Si_{2p} [%]	Al_{2p} [%]	Ca_{2p} [%]
HMDS	57.4 ± 0.5	38.6 ± 0.3	0.93 ± 0.07	0.23 ± 0.07	1.30 ± 0.05
blank	58.3 ± 0.1	38.9 ± 0.1	0.17 ± 0.05	0.20 ± 0.06	1.20 ± 0.04

6.5 PDA measurements

The comparison of all PDA measurements of the different modified paper sheets is depicted in Figure 40. The wetting time (t_w) is defined as the time when the ultrasound intensity reaches 100 % and the penetration speed is calculated from the slope of the measurement curves [72]. A distinction was made to calculate the penetration speed between hydrophobized paper sheets, where the slope is determined from t_w to one second after t_w and the highly absorbing untreated UNUT paper, where the slope is determined from t_w to 200 ms after t_w [72].

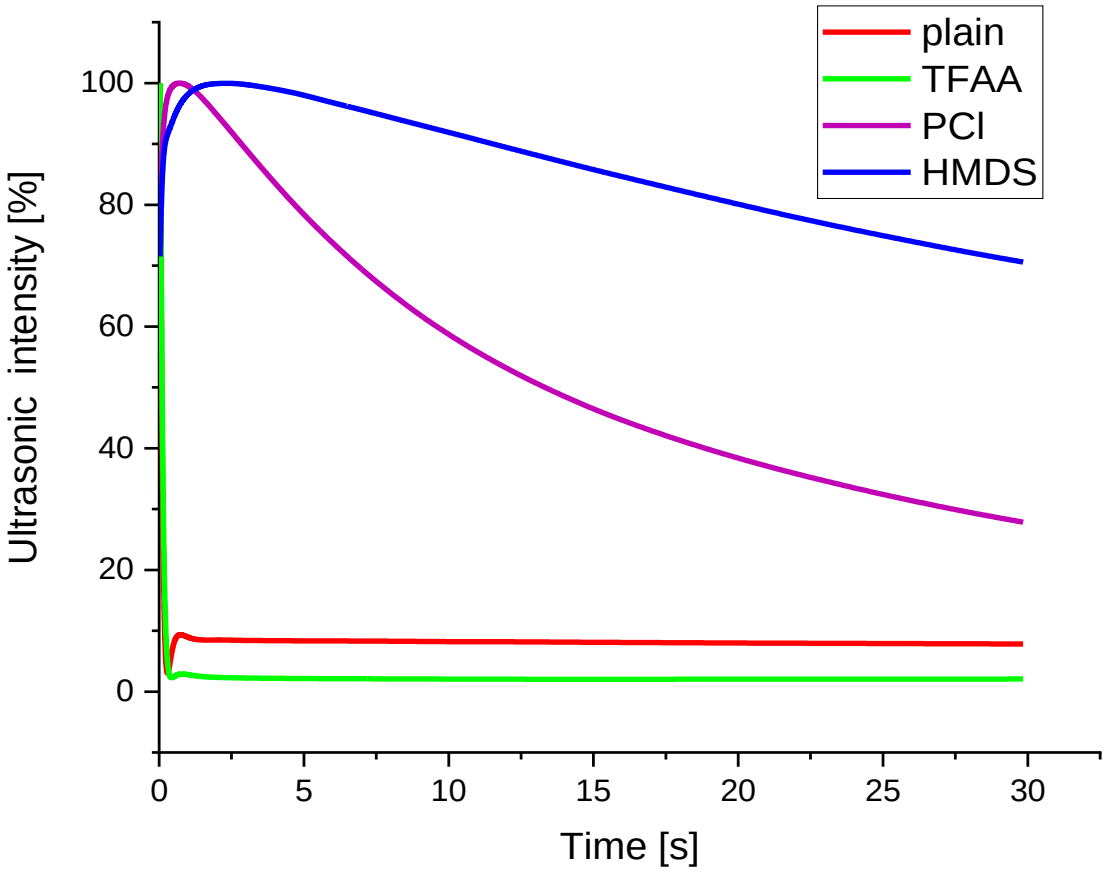

Figure 40: PDA measurements of the different modified paper sheets.

The ultrasound intensity is decreasing after t_w at a constant rate, which indicates a hydrophobization throughout the HMDS modified paper sheet. This also confirms the assumption from the gas-phase hydrophobization with the mask, made from aluminum foil, that the HMDS diffuses through the pore system of the paper and silylates the surface of all fibers. On the other hand, the PDA curve of the palmitoylated paper sheet might indicate that there is only a hydrophobization of the paper surface, because the slope is not decreasing at a constant rate.

The paper that has been treated with an anhydride mixture, shows nearly no differences to the untreated paper. This may be due to the acidic reaction conditions during the hydrophobization, which damage the paper matrix. Therefore, the liquid can penetrate the paper more easily due to the higher roughness and the changed pore structure, although the initial contact angle on the modified paper sheet increased.

In Table 4 the measured wetting times (t_w) and the penetration speed of H_2O of the different modified paper sheets can be seen.

Table 4: Measured wetting time (t_w) and calculated penetration speed of the different modified paper sheets.

	t_w [s]	Penetration speed [1/s]
Plain UNUT	0.03 ± 0.00	537 ± 18
TFAA/Ac_2O	0.03 ± 0.00	442 ± 15
PCl	0.70 ± 0.05	1.54 ± 0.04
HMDS	2.29 ± 0.12	0.42 ± 0.01

6.6 Printing tests of HMDS- and TFAA/Ac_2O-modified samples

The printing quality and drying time of an ink on a paper sheet are some of the most relevant properties in High-Speed Inkjet printing. Therefore, a color density test of the different modified papers was carried out and in Figure 41 (plain UNUT), Figure 42 (HMDS-modified paper) and Figure 43 (TFAA/Ac_2O modified paper) the different printouts are shown. The mean color density values are depicted in Figure 44.

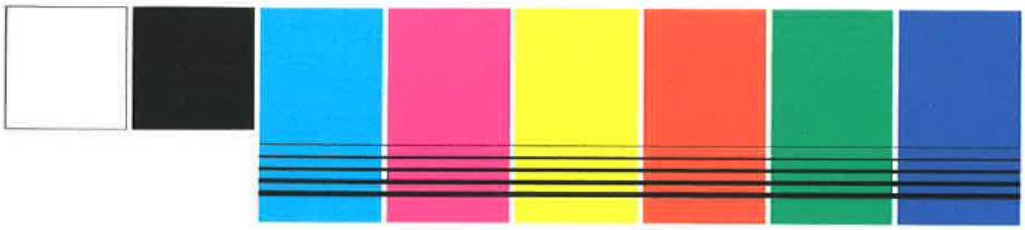

Figure 41: Printout for the color density test on a plain UNUT paper sheet.

Figure 42: Printout for the color density test on a HMDS-modified paper sheet.

Figure 43: Printout for the color density test on an TFAA/Ac_2O modified paper sheet.

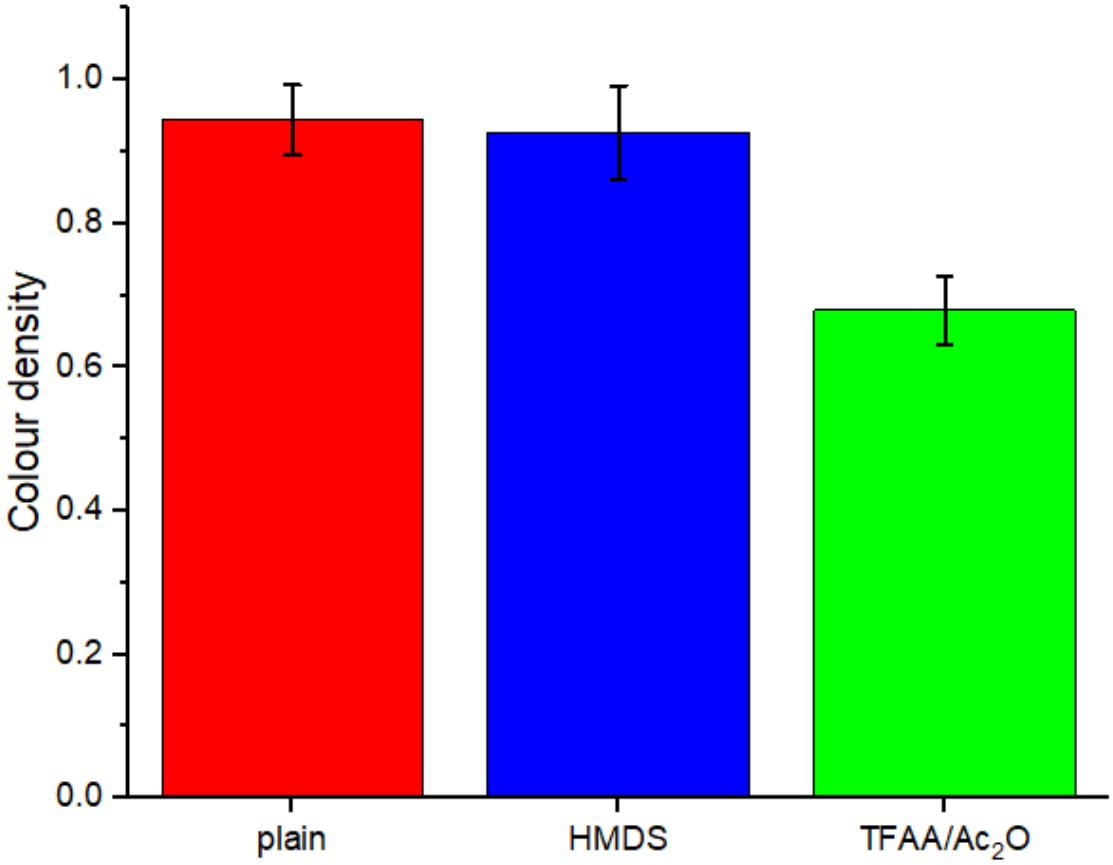

Figure 44: Mean color density values of the printed areas (black, cyan, magenta, yellow, red, green and blue) of the tested paper samples.

Even with the naked eye one can see the big difference in color density of the TFAA/Ac_2O modified sample in comparison to the HMDS-modified and plain UNUT sample. The color density of the HMDS-modified sample, 0.93 ± 0.06, is about the same as the color density of the plain paper sample, which amounts to 0.94± 0.05. The low color density of the TFAA/Ac_2O modified sample, which amounts to 0.68 ± 0.05, is caused by incomplete ink coverage of the sample, which is also visible in microscopic images. This might be caused by a chemical interaction between the ink or the ink pigments with the modified paper surface. Due to the acidic reaction conditions and the formation of bivalent calcium-ions on the surface ($CaCO_3$ reaction in acidic

environment) it might be that the ink dispersion gets destabilized [1]. This mechanism is used specifically in printing to increase the color density. However, it is important to use a suitable amount of ink, since the spreading of the drops is also reduced. [1]

The reason for the lower color density on a TFAA/Ac_2O modified paper sheet can also be seen in microscopic pictures, depicted in Figure 45 and Figure 46.

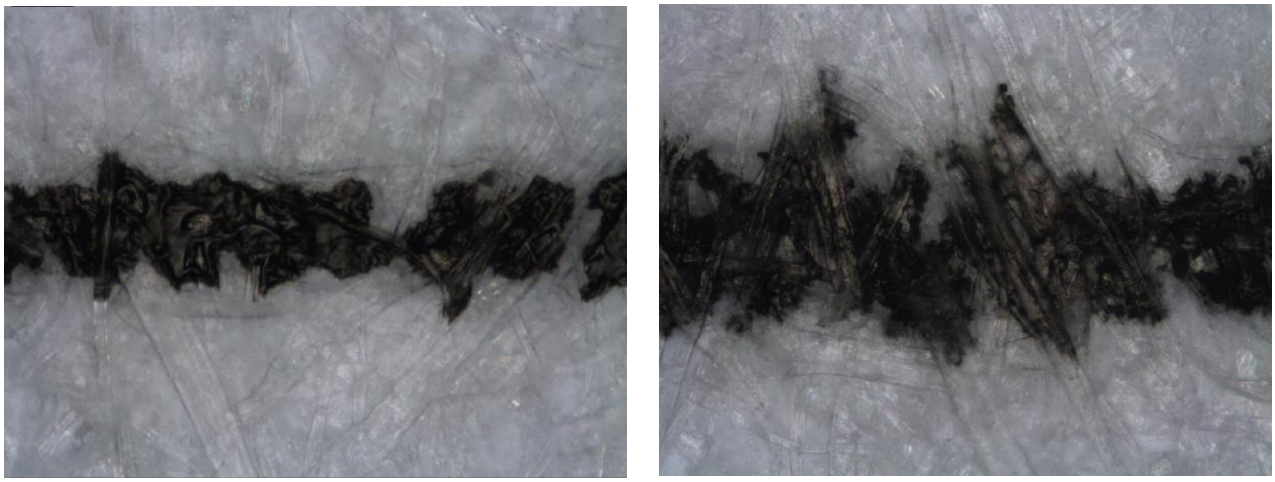

Figure 45: Microscopic images of black printed lines on paper sheets. Left: TFAA/Ac_2O modified paper sheet; Right: plain UNUT paper sheet.

Due to the fixation of the dyes in the ink, the printed ink drops do not merge anymore. Parts of the paper are still unprinted, which leads to lower color densities. In addition, no feathering can be seen on the TFAA/Ac_2O modified paper sample compared to the plain UNUT sample. Feathering is defined as a defect in printouts, whereby uneven and ragged edges are formed due to ink spreading across the surface along the fibers instead of ink penetration into the bulk [82].

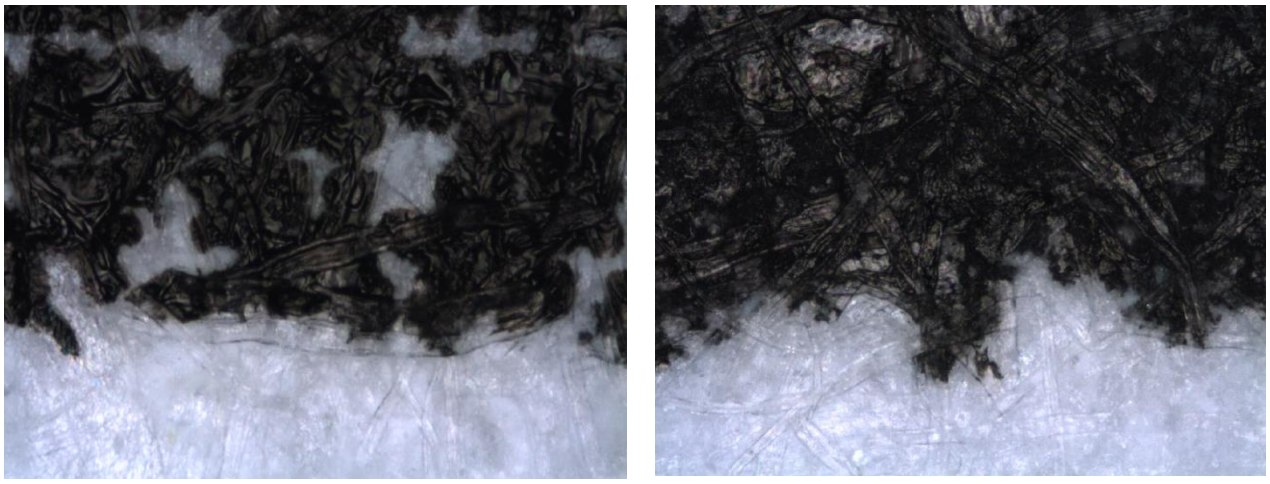

Figure 46: Microscopic images of the border area of a printed black rectangular. Left: TFAA/Ac_2O modified paper sheet; Right: plain UNUT paper sheet.

Taking a closer look at the microscopic images of the HMDS-modified paper sheet (Figure 47 and Figure 48), one can see no differences in ink distribution. The ink drops are merging on the paper surface and a uniform ink distribution is visible. Moreover, less feathering is occurring due to the hydrophobicity of the modified paper surface compared to the plain UNUT sample.

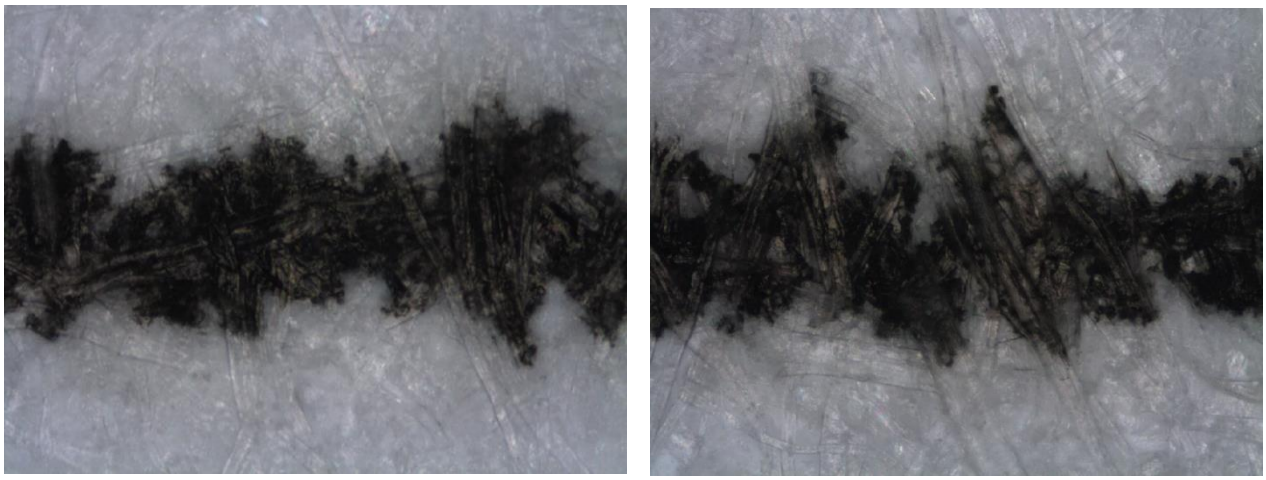

Figure 47: Microscopic images of black printed lines on paper sheets. Left: HMDS modified paper sheet; Right: plain UNUT paper sheet.

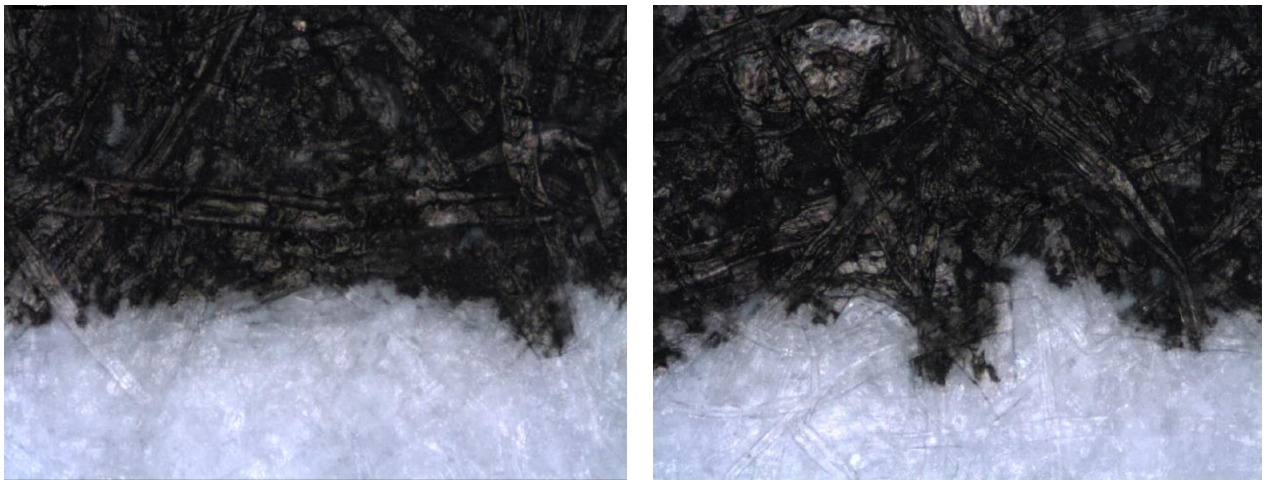

Figure 48: Microscopic images of the border area of a printed black rectangular. Left: TFAA/Ac_2O modified paper sheet; Right: plain UNUT paper sheet.

The results of the smearing tests are visualized in Figure 49. The color density values are representing the smearing tendency and a high color density value is corresponding to a high smearing tendency. The smearing tendency of the TFAA/Ac_2O modified paper sheet is very high, which could be explained by the fixation of the ink dyes on the paper surface leading to impaired ink penetration. Due to the hindered penetration, ink drying is slowed down and smearing is increased. The same effects can be seen with

the use of a primer, for instance $CaCl_2$, which fixates the ink pigments on the paper surface [74]. The color density on the counter paper amounts to 0.52 ± 0,10 on the TFAA/Ac_2O modified paper sheet compared to 0.14 ± 0.02 on the plain UNUT sheet. The high value of the confidence interval is due to the high difference in ink distribution on the counter paper.

On the contrary, the smearing tendency of the HMDS-modified paper sheet is slightly lower than on the plain paper. The color density amounts to 0.12 ± 0.02 compared to 0.14 ± 0.02. This result is not expected, because normally the smearing tendency should increase with a higher hydrophobization degree due to the slower penetration of the ink solvent into the paper. One reason for the fast penetration may be the low surface tension of the black test ink, which amounts to 32 mN/m compared to H_2O which has a surface tension of 72 mN/m at 20 °C. Due to the low surface tension of the ink, the hydrophobization might not have such a big impact on the ink's penetration behavior. Another explanation may be that the penetration is slowed down due to the hydrophobization of the paper sheet, but it cannot be seen with this test assembly. The smearing tendency is measured 10 seconds after the printout is finished and it might be that the penetration of the ink is finished after this time.

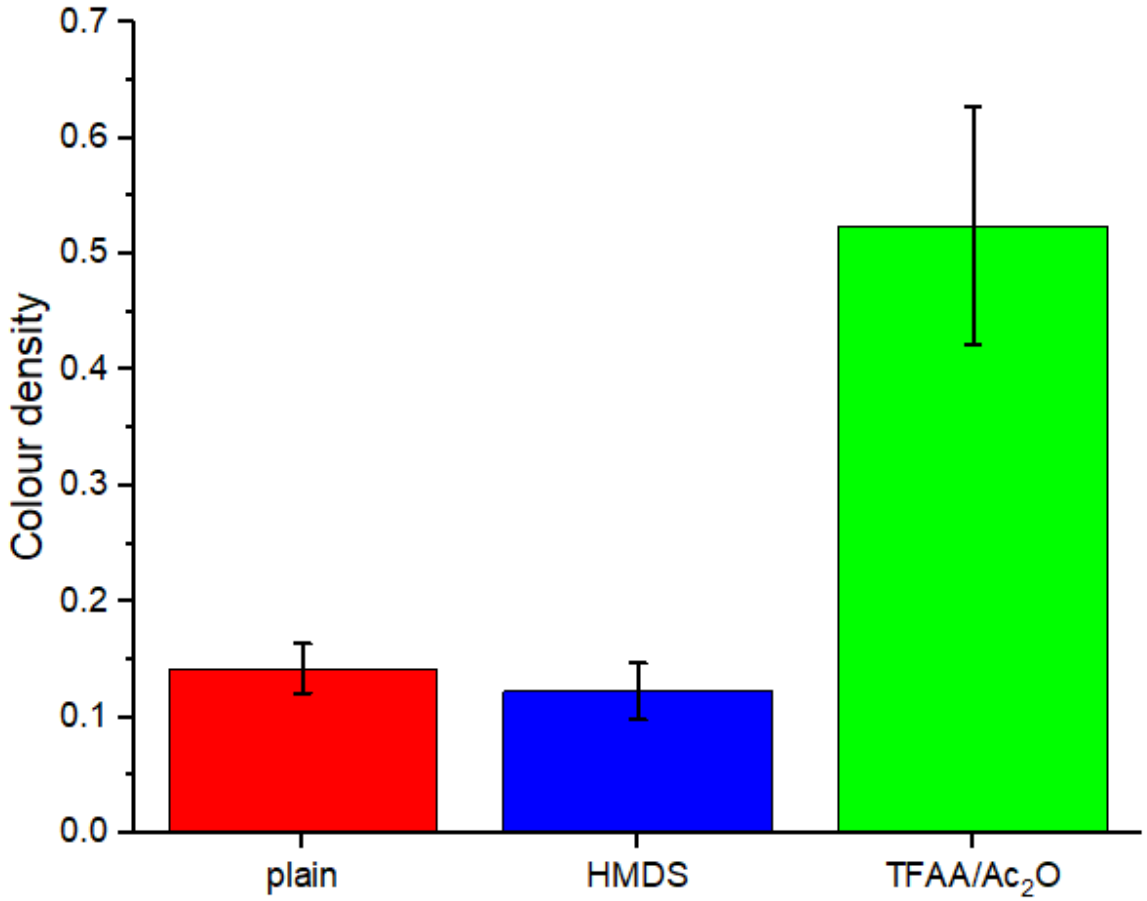

Figure 49: Color densities of the counter paper after the smearing test with a rectangular finger tester.

7 Conclusion

The aim of this master's thesis was to find a method to hydrophobize plain UNUT paper sheets, without changing the pore structure of the paper matrix or any other fundamental paper properties. Therefore, gas-phase hydrophobization with different chemicals was used and the paper was analyzed afterwards to detect occurring changes of the paper properties after the modification.

Plain UNUT paper was hydrophobized with ASA, palmitoyl chloride, an TFAA/AcOH and TFAA/Ac_2O mixture and with HMDS. To check the hydrophobization contact angle measurements were carried out. All methods except the ASA-deposition worked well. The highest contact angle was achieved with the gas-phase hydrophobization with palmitoyl chloride, but because of the high reaction temperature and the low pressure needed to evaporate the reactant no further research was carried out.

The gas-phase esterification with a mixture of TFAA and Ac_2O led to higher contact angles compared to the unsized raw paper and therefore a higher hydrophobization of the paper surface, but due to the very acidic reaction conditions the mechanical properties, especially the tensile strength, was lowered. The printing tests showed that the modified paper surface behaves similarly to a paper coated with a primer, for instance $CaCl_2$. The primer-like effect is visible in an increased smearing tendency and a lower color density, because of the enhanced fixation of the ink pigments on the paper surface. Due to the primer-like effect a higher amount of ink should be used to obtain a higher color density because of the reduced spreading of the drops.

All in all, the gas-phase silylation with HMDS led to the best results, since the paper was hydrophobized, but neither the mechanical nor the optical properties were changed in the process. Moreover, a mercury porosimetry measurement also confirmed that the porosity of the sample did not change during the modification. It was also shown by PDA measurements and a mask test, that HMDS diffuses through the pore system and thus the surface of each fiber, even in the bulk of the paper is made hydrophobic.

Due to the results, especially of the HMDS-modification, further investigations on the change of the hydrophobicity with various paper types with different porosities can be carried out.

8 Outlook

To investigate the wettability and penetration effects on paper sheets with different degrees of hydrophobization and different porosities, a larger reactor for the gas-phase hydrophobization had to be developed. For this purpose, a plexiglass box was made, in which up to ten sheets of paper can be modified simultaneously. The sketch, as well as the finished box are depicted in Figure 50 and Figure 51.

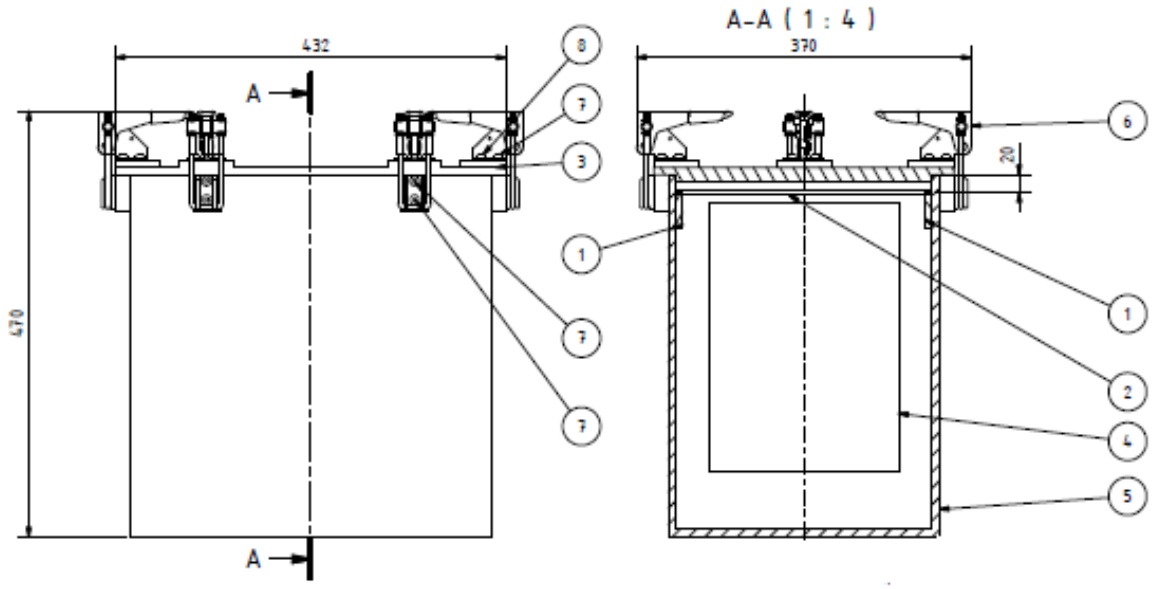

Figure 50: Sketch of the plexiglass box: 1) brackets for aluminum bars; 2) aluminum bars; 3) lid; 4) paper sheet; 5) body of the box; 6) latch clamps; 7) and 8) ISO 7380-1 M6 x 16 and ISO 7380-1 M6 x 12.

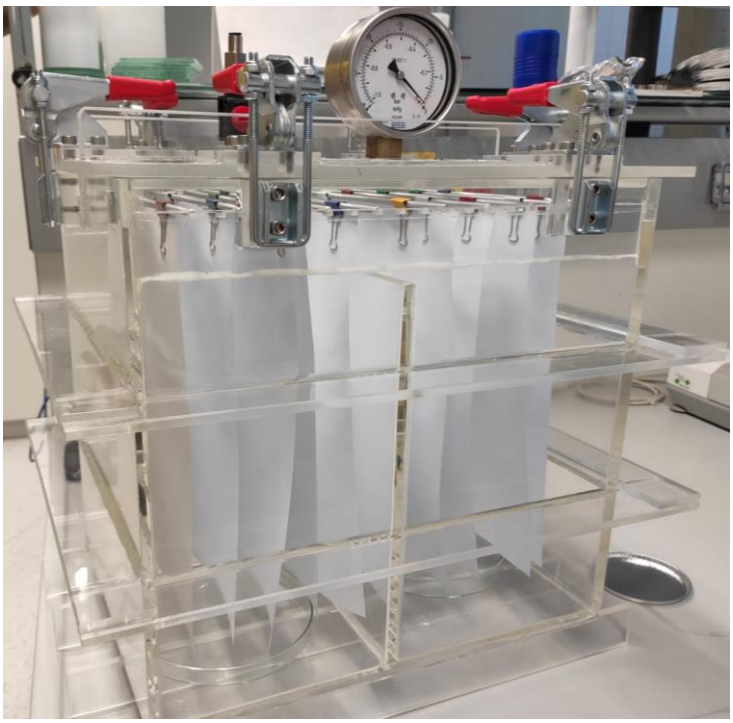

Figure 51: Plexiglas box for scale-up experiments with HMDS.

Unfortunately, the box could not withstand the vacuum of 400 mbar and cracked at various places, although it was reinforced with several struts around and inside the whole vacuum chamber. Therefore, an aluminum vacuum chamber was ordered to carry out the gas-phase hydrophobization with HMDS on a larger scale.

In addition, the results were submitted to the Journal Int. J. Biological Biomacromolecules as a publication. The publication is still under review.

9 Abbreviations

UNUT	Untreated and unsized paper
AKD	Alkyl ketene dimers
ASA	Alkenyl succinic acid
TFAA	Trifluoroacetic anhydride
Ac_2O	Acetic anhydride
AcOH	Acetic acid
HMDS	Hexamethyldisilazane
PDA	Penetration dynamics analyzer
ATR-IR	Attenuated-total-reflectance infrared spectroscopy
CA	Contact angle

10 List of figures

11 Bibliography

[1] S. Magdassi, *The Chemistry of Inkjet Inks*. Singapore: World Scientific Publishing, 2010.

[2] S. Sousa, J. A. Gamelas, A. De Oliveira Mendes, P. T. Fiadeiro, and A. Ramos, "Interactions of ink colourants with chemically modified paper surfaces concerning inkjet print improvement," *Mater. Chem. Phys.*, vol. 139, no. 2–3, pp. 877–884, 2013.

[3] H. Hamada and D. Bousfield, "Effect of Cationic Additives on Ink Penetration," *J. Pulp Pap. Sci.*, vol. 35, pp. 118–122, 2009.

[4] M. A. Hubbe, "Paper's resistance to wetting - A review of internal sizing chemicals and their effects," *BioResources*, vol. 2, no. 1, pp. 106–145, 2007.

[5] O. B. Wurzburg and E. D. Mazzarella, "Novel paper sizing process," US3,102,064, 1963.

[6] L. Göttsching and C. Katz, *Papier-Lexikon*. Gernsbach: Deutscher Betriebswirte-Verlag, 1999.

[7] J. Blechschmidt and S. Heinemann, *Taschenbuch der Papiertechnik*. München: Carl Hanser Verlag, 2013.

[8] H. Holik, *Handbook of Paper and Board*. Weinheim: Wiley-VCH, 2006.

[9] Verband Deutscher Papierfabriken e.V., "Papier Kompass 2016," p. 2, 2016.

[10] C. J. Biermann, *Handbook of Pulping and Papermaking*, 2nd ed. San Diego: Academic Press, 1996.

[12] W. E. Scott, *Principles of Wet End Chemistry*. Atlanta: TAPPI Press, 1996.

[13] E. Strazdins, D. F. Zinkel, and J. Russell, *Paper sizes and sizing*. New York: Pulp Chemical Association, 1989.

[14] M. Hubbe, "Acidic and alkaline sizings for printing, writing, and drawing papers," *Pap. Gr. Annu.*, vol. 23, pp. 139–151, 2004.

[15] T. D. Barrett, *Early european papers / contemporary conservation papers: A report from fall 1984 through fall 1987*. London: The Paper Conservator, 1989.

[16] J. S. Arney and C. A. H., “A kinetic study of the influence of acidity on the accelerated aging of paper.,” *Chem. Soc., Advan. Chem. Ser.*, vol. 193, no. 14, pp. 189–204, 1981.

[17] A. F. Nitzman and A. T. Royappa, “Sizing variations of dispersed rosin sizes with fortification, hardness, pH, and temperature,” *Tappi J.*, vol. 2, no. 4, pp. 8–11, 2003.

[18] L. Neimo, *Papermaking Chemistry*. Helsinki: Fapet Oy, 1999.

[19] K. T. Hodgson, “A review of paper sizing using alkyl ketene dimer versus alkenyl succinic anhydride,” *Appita*, vol. 47, no. 5, pp. 402–406, 1994.

[20] J. M. Gess and D. S. Rende, “Alkenyl Succinic Anhydride (ASA),” *Tappi J.*, vol. 4, no. 9, pp. 25–30, 2005.

[21] H. L. Lee, J. Y. Shin, C. H. Koh, H. Ryu, D. J. Lee, and C. Sohn, “Surface sizing with cationic starch: Its effect on paper quality and papermaking process,” *Tappi J.*, vol. 1, no. 3, pp. 34–40, 2002.

[22] S. Porkert, “Physico-Chemical Processes during Reactive Paper Sizing with Alkenyl Succinic Anhydride (ASA),” Dissertation: Technische Universität Dresden, 2016.

[23] J. Kettle, T. Lamminmäki, and P. Gane, “A review of modified surfaces for high speed inkjet coating,” *Surf. Coatings Technol.*, vol. 204, no. 12–13, pp. 2103–2109, 2010.

[24] Hue P. Le, “Progress and Trends in Ink-jet Printing Technology,” *J. Imaging Sci. Technol.*, vol. 42, no. 1, pp. 49–62, 1998.

[25] R. Li, Y. Zhang, Y. Cao, and Z. Liu, “Ink Penetration of Uncoated Inkjet Paper and Impact on Printing Quality,” *BioResources*, vol. 10, no. 4, pp. 8135–8147, 2015.

[26] P. Emmel and R. D. Hersch, “Modeling ink spreading for color prediction,” *J. Imaging Sci. Technol.*, vol. 46, no. 3, pp. 237–246, 2002.

[27] T. Kishida, A. Kouichirou, T. Fukui, and S. Kanou, “Influence of coating pore structure and ink set property on ink dryback in sheet-fed offset printing,” TAPPI Coating Conference and Trade Fair, San Diego, CA, United States, 2001.

[28] P. J. Heard, J. S. Preston, D. J. Parsons, J. Cox, and G. C. Allen, “Visualisation of the distribution of ink components in printed coated paper using focused ion beam techniques,” *Colloids Surfaces A Physicochem. Eng. Asp.*, 2004.

[29] T. Young, “An Essay on the Cohesion of Fluids.,” *Philiosophical Trans. R. Soc. London*, vol. 95, no. 65, 1805.

[30] “Krüss - Contact angle.” [Online]. Available: https://www.kruss-scientific.com/services/education-theory/glossary/contact-angle/. [Accessed: 20-Jan-2020].

[31] G. Wedler, *Lehrbuch der Physikalischen Chemie*. Weinheim: Wiley-VCH, 2012.

[32] “Rame-Hart - Contact Angle.” [Online]. Available: http://www.ramehart.com/contactangle.htm. [Accessed: 11-Jan-2020].

[33] A. Marmur, “Wetting on hydrophobic rough surfaces: To be heterogeneous or not to be?,” *Langmuir*, vol. 19, no. 20, pp. 8343–8348, 2003.

[34] D. Quéré, “Wetting and Roughness,” *Annu. Rev. Mater. Res.*, vol. 38, no. 1, pp. 71–99, 2008.

[35] K. Y. Law and H. Zhao, *Surface wetting: Characterization, contact angle, and fundamentals*. Heidelberg: Springer International Publishing Switzerland, 2015.

[36] R. N. Wenzel, “Resistance of solid surfaces to wetting by water,” *Ind. Eng. Chem.*, vol. 28, no. 8, pp. 988–994, 1936.

[37] B. D. Cassie, A. B. D. Cassie, and S. Baxter, “Of porous surfaces,” *Trans. Faraday Soc.*, vol. 40, no. 5, pp. 546–551, 1944.

[38] S. Han, R. Yang, C. Li, and L. Yang, “The wettability and numerical model of different silicon microstructural surfaces,” *Appl. Sci.*, vol. 9, no. 3, 2019.

[39] M. Nosonovsky, “On the range of applicability of the Wenzel and Cassie equations,” *Langmuir*, vol. 23, no. 19, pp. 9919–9920, 2007.

[40] A. Marmur and E. Bittoun, “When wenzel and cassie are right: Reconciling local and global considerations,” *Langmuir*, vol. 25, no. 3, pp. 1277–1281, 2009.

[41] L. Gao and T. J. McCarthy, “How Wenzel and Cassie were wrong,” *Langmuir*, vol. 23, no. 7, pp. 3762–3765, 2007.

[42] C. W. Extrand, “Contact angles and hysteresis on surfaces with chemically heterogeneous islands,” *Langmuir*, vol. 19, no. 9, pp. 3793–3796, 2003.

[43] F. E. Bartell and J. W. Shepard, “Surface roughness as related to hysteresis of contact angles. II. The systems paraffin-3 molar calcium chloride solution-air and paraffin-glycerol-air,” *J. Phys. Chem.*, vol. 57, no. 4, pp. 455–458, 1953.

[44] G. McHale, “Cassie and Wenzel: Were they really so wrong?,” *Langmuir*, vol. 23, no. 15, pp. 8200–8205, 2007.

[45] A. Dupre, *Theorie Mécanique de la Chaleur*. Gauthier-Villars, 1869.

[46] “Krüss - Work of adhesion.” [Online]. Available: https://www.kruss-scientific.com/services/education-theory/glossary/work-of-adhesion/. [Accessed: 13-Jan-2020].

[47] N. K. Adam, “Use of the Term ‘Young’s Equation’ for Contact Angles,” *Nature*, vol. 180, pp. 809–810, 1957.

[48] M. E. Schrader, “Young-Dupre Revisited,” *Langmuir*, vol. 11, no. 9, pp. 3585–3589, 1995, doi: 10.1021/la00009a049.

[49] D. K. Owens and R. C. Wendt, “Estimation of the surface free energy of polymers,” *J. Appl. Polym. Sci.*, vol. 13, no. 8, pp. 1741–1747, 1969.

[50] W. Rabel, “Einige aspekte der Benetzungstheorie und ihre Anwendung auf die Untersuchung und Veränderung der Oberflächeneigenschaften von Polymeren,” in *Farbe und Lacke*, 1971, pp. 997–1005.

[51] D. H. Kaelble, “Dispersion-Polar Surface Tension Properties of Organic Solids,” *J. Adhes.*, vol. 2, no. 2, pp. 66–81, 1970.

[52] “Krüss - Methode nach Owens, Wendt, Rabel und Kaelble (OWRK).” [Online]. Available: https://www.kruss-scientific.com/de/service/schulung-theorie/glossar/methode-nach-owens-wendt-rabel-und-kaelble-owrk/. [Accessed: 13-Jan-2020].

[53] F. M. Fowkes, “Determination of interfacial tensions, contact angles, and dispersion forces in surfaces by assuming additivity of intermolecular interactions in surfaces,” *J. Phys. Chem.*, vol. 66, no. 2, p. 382, 1962.

[54] S. Krainer, “Investigation of Liquid Penetration and Wetting on Paper in the

High Speed Inject Field," Dissertation: Graz University of Technology, 2019.

[55] F. M. Fowkes, "Attractive Forces At Interfaces," *Ind. Eng. Chem.*, vol. 56, no. 12, pp. 40–52, 1964.

[56] "Dataphysics Instruments - Bestimmung der Oberflächenenergie eines Festkörpers." [Online]. Available: https://www.dataphysics-instruments.com/de/wissen/grenzflaechen-verstehen/festkoerper-oberflaechenenergie/. [Accessed: 14-Jan-2020].

[57] E. Washburn, "Note on the dynamics of capillary flow," *Phys. Rev.*, vol. 18, no. 3, pp. 206–209, 1921.

[58] A. Adamson, *A Text-Book of Physical Chemistry*. London: Academic Press, Inc., 1973.

[59] S. Smirnov, I. Vlassiouk, P. Takmakov, and F. Rios, "Water confinement in hydrophobic nanopores. Pressure-induced wetting and drying," *ACS Nano*, vol. 4, no. 9, pp. 5069–5075, 2010.

[60] R. Lucas, "Üeber das Zeitgesetz des kapillaren Aufstiegs yon Flüssigkeiten.," *Kolloid-Zeitschrift*, vol. 23, no. 1, pp. 15–22, 1918.

[61] B. D. MacDonald, "Flow of liquids through paper," *J. Fluid Mech.*, vol. 852, pp. 1–4, 2018, doi: 10.1017/jfm.2018.536.

[62] M. M. Gong and D. Sinton, "Turning the Page: Advancing Paper-Based Microfluidics for Broad Diagnostic Application," *Chem. Rev.*, vol. 117, no. 12, pp. 8447–8480, 2017, doi: 10.1021/acs.chemrev.7b00024.

[63] A. S. H. Makhlouf and I. Tiginyanu, *Nanocoatings and ultra-thin films: Technologies and applications*. Cambridge: Woodhead Publishing, 2011.

[64] K. L. Choy, "Chemical vapour deposition of coatings," *Prog. Mater. Sci.*, vol. 48, no. 2, pp. 57–170, 2003.

[65] D. M. Dobkin and M. K. Zuraw, *Principles of Chemical Vapor Deposition*. Dordrecht: Springer Science+Business Media, B.V., 2003.

[66] K. E. Spear, "Principles and applications of chemical vapor deposition (CVD)," *Pure Appl. Chem.*, vol. 54, no. 7, pp. 1297–1311, 1982.

[67] X. Yongdong and Y. Xiu-Tian, *Chemical Vapour Deposition - An Integrated Engineering Design for Advanced Materials*. London: Springer, 2010.

[68] H. O. Pierson, *Handbook of Chemical Vapor Deposition (CVD)*. New York: Noyes Publications/ William Andrew Publishing, 1999.

[69] W. O. Filtvedt, A. Holt, P. A. Ramachandran, and M. C. Melaaen, "Chemical vapor deposition of silicon from silane: Review of growth mechanisms and modeling/scaleup of fluidized bed reactors," *Sol. Energy Mater. Sol. Cells*, vol. 107, pp. 188–200, 2012.

[70] A. Sherman, *Chemical Vapor Deposition For Microelectronics - Principles, Technology and Applications*. New Yersey: Noyes Publications.

[71] A. Ryoki, Tobe; Sekiguchi and S. Masao, "Plasma enhanced CVD apparatus, plasma enhanced processing apparatus and plasma enhanced CVD method," US 5,855,685, 1999.

[72] K. Sarah and H. Ulrich, "RSC Advances sheets measured with ultrasound , direct absorption," *RSC Adv.*, vol. 8, pp. 12861–12869, 2018.

[73] "Hg-porosimetry - University of Duisburg." [Online]. Available: https://www.uni-due.de/materials/HG_Druck.shtml. [Accessed: 02-Mar-2020].

[74] C. Waldner, "Einflüsse auf das Trocknungsverhalten der Druckfarbe beim High Speed Inkjet Druck," Master´s Thesis: Graz Technical University, 2019.

[75] H. Zhang, D. Kannangara, M. Hilder, R. Ettl, and W. Shen, "The role of vapour deposition in the hydrophobization treatment of cellulose fibres using alkyl ketene dimers and alkenyl succinic acid anhydrides," *Colloids and Surfaces: A Physicochemical and Engineering Aspects*, vol. 297, no. 1–3, pp. 203–210, 2007.

[76] J. Weigert, "Untersuchung zur chem. Modifizierung von Zellstoff zur Verminderung der Verhornungsneigung sowie zu den sich daraus ergebenden papiertechnologischen Eigenschaften," Dissertation: Technical University Darmstadt, 1999.

[77] V. Hospodarova, E. Singovszka, and N. Stevulova, "Characterization of Cellulosic Fibers by FTIR Spectroscopy for Their Further Implementation to Building

Materials," *Am. J. Anal. Chem.*, vol. 09, no. 06, pp. 303–310, 2018.

[78] G. David *et al.*, "Exploring the potential of gas-phase esterification to hydrophobize the surface of micrometric cellulose particles," *Eur. Polym. J.*, vol. 115, no. September 2018, pp. 138–146, 2019.

[79] R. L. Redington and K. C. Lin, "Infrared spectra of trifluoroacetic acid and trifluoroacetic anhydride," *Spectrochim. Acta Part A Mol. Spectrosc.*, vol. 27, no. 12, pp. 2445–2460, 1971.

[80] G. Chinga-Carrasco *et al.*, "Bleached and unbleached MFC nanobarriers: Properties and hydrophobisation with hexamethyldisilazane," *J. Nanoparticle Res.*, vol. 14, no. 12, pp. 1–10, 2012.

[81] M. Schaub, G. Wenz, G. Wegner, A. Stein, and D. Klemm, "Ultrathin films of cellulose on silicon wafers," *Adv. Mater.*, vol. 5, no. 12, pp. 919–922, 1993.

[82] "Feathering - Labelplanet UK." [Online]. Available: https://www.labelplanet.co.uk/glossary-of-label-terms/feathering.php. [Accessed: 24-Feb-2020].